ELSEVIER

Contents lists available at ScienceDirect

Deep-Sea Research Part I

journal homepage: www.elsevier.com/locate/dsri



Coccolithophore distributions of the North and South Atlantic Ocean



William M. Balch*, Bruce C. Bowler, David T. Drapeau, Laura C. Lubelczyk, Emily Lyczkowski, Catherine Mitchell, Amy Wyeth¹

Bigelow Laboratory for Ocean Sciences, 60 Bigelow Drive, POB 380, East Boothbay, ME, 04544, USA

ARTICLE INFO

Keywords:
Coccolithophores
Particulate inorganic carbon
Diversity
Great calcite belt
Biogenic silica
Subantarctic mode water

ABSTRACT

We present average coccolithophore and associated biogeochemical results from ten Atlantic Meridional Transect (AMT) cruises between 50°N-50°S, results that show a number of unique observations across this massive data set. Lowest concentrations of coccolithophores were consistently found in equatorial waters. Highest concentrations of coccolithophore cells and coccoliths were associated with temperate, sub-polar environments. Concentrations of detached coccoliths were dispersed to ~ 300 m depth and show low inter-cruise variance. Coccolithophore cell concentrations in the subtropics remain highest at < 200m depth in the S. Atlantic and 100m in the N. Atlantic, near the 26.5 to 27 sigma-theta (σ_{θ}) isopycnal, within the Subantarctic Mode Water (SAMW). Diversity and species richness of coccolithophore cells was greater than for the detached coccoliths and generally greater in surface populations than in the deep chlorophyll maximum (DCM). Placolithbearing coccolithophore species dominated over the umbelliform and floriform coccolithophore groups in surface waters of the Southern Ocean at 50°S, as well as the DCM from 50°S to the equator. The DCM was strongly associated with the $\sigma_{\theta},$ of $\sim\!27\,\text{kg}\,\text{m}^{\text{-}3},$ coincident with the top of the nitracline, within the SAMW. Concentrations of coccolithophore cells and detached coccoliths were much less related to the density field than chlorophyll was. Highest integrated euphotic coccolith concentrations were observed when the integrated POC:chlorophyll ratio was highest. PIC:POC ratios increased with depth and approached maximum values near the top of the nitracline. Great Calcite Belt waters (upper 300m) showed biogenic silica:particulate inorganic carbon ratios (BSi:PIC) > 1 while all other waters showed BSi:PIC ratios < 1. Peaks in PIC and BSi were observed within, and above the SAMW, in waters with low phosphate and silicate concentrations. The results of this study suggest that coccolithophore-rich SAMW in the Southern Ocean is being conditioned after its formation, such that by the time it upwells in the Atlantic equatorial region, the water is no longer conducive to coccolithophore growth.

1. Introduction

1.1. Coccolithophore ecology

Coccolithophores are single-celled calcifying algae of the phylum (or division) Haptophyta and class Prymnesiophyceae that produce calcite scales, called coccoliths. Both the coccolithophores and their detached coccoliths are ubiquitously found in the surface waters throughout the global ocean. They are influential on ocean biogeochemistry due to their dense calcite which provides ballast for sinking organic debris plus they help drive the biological carbon pump and alkalinity pump (Riebesell et al., 2009). They also have a strong impact on the optical properties of seawater (particularly back-scattering) due to the high refractive index of calcite and these

properties are important for their remote detection by satellite (Balch, 2018). However, the backscattering properties of coccoliths vary as a function of species, size and shape (Balch et al., 1999; Fournier and Neukermans, 2017; Gordon and Du, 2001), all of which are highly variable across the entire Atlantic basin.

There have been a number of key basin-scale studies of coccolithophores, their distributions in the pelagic realm as well as in the sediments (Hagino et al., 2000; McIntyre and Be, 1967; Okada and Honjo, 1973a, b; Okada and McIntyre, 1977, 1979). Indeed, much of what we know about coccolith distributions in sediments was based on a number of early studies (Andreé, 1920; Deflandre and Fert, 1952, 1954; Gaarder, 1954; Lohmann, 1902, 1908). There also has been considerable work on their pelagic distributions, taxonomy, biology, physiology and ecology summarized in various works (Balch, 2018;

E-mail address: bbalch@bigelow.org (W.M. Balch).

^{*} Corresponding author.

¹ Current Address: University of Washington, School of Oceanography, Box 357940, Seattle, WA 98195-7940, USA

Green and Leadbeater, 1994; Poulton et al., 2017; Taylor et al., 2017; Thierstein and Young, 2004; Winter and Siesser, 1994). While there is generally a good correspondence between the relative species abundance of coccolithophores in oceans and sediments (Baumann et al., 2004; Ziveri et al., 2004), there is a slightly broader geographic distribution of various coccolithophore species in the pelagic realm than in the sediments (McIntyre and Be, 1967).

Coccolithophore species occupy three important niches in the sea in shallow and deep waters. Young (1994) defined three general ecological groupings of coccolithophores, each associated with three distinct environments: (1) placolith-bearing cells such as *Emiliania huxleyi*, found in shelf or mid-ocean upwelling regions, (2) umbelliform cells such as *Umbellosphaera tenuis*, found in more oligotrophic, nutrient-depleted waters and (3) floriform cells such as *Florisphaera profunda*, which are associated with deep photic-zone assemblages in low to midlatitudes (see also Boeckel and Baumann (2008)). Moreover, Young (1994) discussed the appearance of motile cells within the placolith-bearing group; flagellae could substantially enhance the ability of coccolithophores to exploit stratified, nutrientpoor environments.

Coccolithophores represent a highly diverse class of phytoplankton, whether measured using a conventional diversity index (like the Shannon Weiner index (H')) or the most simple index of diversity, the numbers of species (or species richness, S) (Magurran, 2004). At the HOTS (Hawaiian Ocean Time Series) station in the subtropical North Pacific, a total of 125 species of coccolithophores (along with 19 previously undescribed species) were enumerated in a two-year study using scanning electron microscopy (SEM), with as many as 58 species found in one sample (Cortés et al., 2001). These 125 species represented 63% of all the known extant coccolithophore species (199 in total) (Jordan and Kleijne, 1994). Contrasting this high species richness is low species evenness (J') (Magurran, 2004), with only five species contributing ~30% of the total coccolithophore community. In the subtropical North Atlantic, 60 coccolithophore species were observed using light microscopy (which is less reliable for coccolithophore classification to the species level than SEM) (Haidar and Thierstein, 2001). Nonetheless, of those 60 species, only six comprised 89% of the community and 44 species comprised < 2% of the community, again emphasizing the very low species evenness of subtropical Atlantic coccolithophore communities (Thierstein et al., 2004). In contrast, Poulton et al. (2017) described the coccolithophores from the equatorial and subtropical Atlantic, and within 199 samples, they observed 171 species of coccolithophores, with 140 representing < 5% of total cell numbers. The result is that most coccolithophore species are so rare that they are not observed in cell count samples unless large enough volumes are sampled. Such low evenness is similar to other plankton groups, such as copepod zooplankton (McGowan and Walker, 1993); these observations are consistent with the "paradox of the plankton" where high diversity is at odds with ecological models that would predict far fewer co-existing species, based on classic niche partitioning arguments. Fast resource depletion (Li and Chesson, 2016), herbivory (Leibold et al., 2017), and inter-specific variability (Menden-Deuer and Rowlett, 2014) are some of the hypotheses used to explain such high planktonic diversities. Species diversity is also thought to decrease with increasing latitude (Barton et al., 2010).

More recent work has continued to demonstrate this extraordinary diversity within the haptophyte family (which include the coccolithophores) and that both calcifying and non-calcifying haptophytes dominate global phytoplankton standing stock (based on the abundance of their unique accessory pigment, 19'-hexanoyloxyfucoxanthin [19-Hex]) (Liu et al., 2009). Liu et al. (2009) suggest that haptophytes contribute more biomass globally than the photosynthetic prokaryotes, *Prochlorococcus* (Chisholm et al., 1988) and *Synechococcus* (Waterbury et al., 1979) and likely contribute more to global primary production. Liu et al. (2009) propose that the haptophytes contribute some 30-50% of the total standing stock of photosynthetic algae in the world ocean. Further, some floriform coccolithophores live below the standard

euphotic zone, thus extending haptophycean productivity into the subeuphotic regions of the upper water column. Indeed, there is historical evidence for mixotrophy for a few species of coccolithophores (Conrad, 1941; Houdan et al., 2006; Pintner and Provasoli, 1968). That is, they appear to grow on both inorganic and organic carbon sources (Medlin et al., 2008).

1.2. Subantarctic Mode Water and controls on phytoplankton productivity

Subantarctic Mode Water (SAMW) is considered the major source of nutrients extending northward of the 30°S parallel (Sarmiento et al., 2004). It is associated with a pycnostad between potential densities (σ_{θ}) of 26.5 to 27 and forms just to the north of the Subantarctic Front (Cerovečki et al., 2013). It carries low pre-formed silicate and iron due to extensive uptake by diatoms in its region of formation. However, SAMW carries pre-formed nitrate northward as high-nutrient-lowchlorophyll (HNLC) waters, tracking the bottom of the euphotic zone as it moves to the north. This water arrives at the base of the euphotic zone in the Atlantic equatorial upwelling region, giving the region a HNLC character. Cyclonic eddies in overlying waters might also lift this SAMW water vertically; this combined with relative amounts of silicate and nitrate plus HNLC character could further influence the classes of algae that can grow in the overlying water (such as diatoms versus coccolithophores). A similar mechanism was proposed previously by Bibby and Moore (2011) for controlling the diatom abundance in the subtropical North Atlantic and Pacific (except note, they were referring to Si*, the difference between silicate and nitrate). SAMW can be traced well north in the North Atlantic Ocean (McCartney, 1982; Poole and Tomczak, 1999; Sloyan and Rintoul, 2001) and some three quarters of the primary production north of 30°S (including equatorial waters) is hypothesized to be supported by SAMW formation in the Southern Ocean, ultimately originating in the region of the Subantarctic Front (Sarmiento et al., 2004).

The following work is based on the synthesis of previously unpublished results from over a decade of Atlantic Meridional Transect (AMT) cruises between 2004-2015, sampled between north temperate waters and south temperate waters of the Atlantic Ocean. We address several fundamental knowledge gaps about coccolithophores in the Atlantic at basin scales. What is the mean distribution (and variance) of coccolihophores and their detached coccoliths? How is this related to the mean nutrient distributions for these same cruises? How do the ecological indices of coccolithophores and their detached coccoliths (diversity, richness and evenness) vary across the Atlantic basin? How is coccolithophore abundance observed in these cruises related to the biogeochemistry, including particulate inorganic carbon (PIC; associated with coccolithophores), particulate organic carbon (POC; associated with all organic matter, living and detrital), biogenic silica (BSi; associated with mostly diatoms) and chlorophyll concentration (associated with all phytoplankton). We examine variability of coccolithophores and biogeochemical variables as a function of water masses (e.g. SAMW), nutrient chemistry and biogeography to define the overarching factors controlling coccolithophore distributions.

2. Methods

2.1. Regions sampled and water sampling protocols

Abbreviations used in this work are given in Table 1. The data to be presented in this paper were collected on ten AMT cruises between September 2004 and November 2015 between the United Kingdom and either Cape Town, South Africa (cruises 15-17) or Punta Arenas, Chile or Stanley, Falkland Islands (cruises #18-22, 24, 25; Table 2; Fig. 1). All cruises went southwards from the UK except AMT cruise 16 which went northwards from South Africa to the UK. For the cruises ending in South America, water sampling ended just north of the Falkland Islands at $\sim 50\,^{\circ}\mathrm{S}$. Seawater was typically sampled during daily pre-dawn

Table 1 Abbreviations used in this study.

AMT	Atlantic Meridional Transect
BSi	Biogenic Silica
CV	Coefficient of variation
DCM	Deep Chlorophyll Maximum
DIN	Dissolved Inorganic Nitrogen
DIP	Dissolved Inorganic Phosphorus
EQ	Equatorial Water Masses
GCB	Great Calcite Belt
HNLC	High-Nutrients-Low-Chlorophyll
EQ	Equatorial Region
NAG	North Atlantic Gyre
NTW	North Temperate Water
PF	Polar Front
PIC	Particulate inorganic carbon
POC	Particulate organic carbon
SEM	Scanning electron microscopy
SAG	South Atlantic Gyre
SAMW	Sub-Antarctic Mode Water
STW	South Temperate Water
Z _{chlmax}	1% irradiance light depth

(02:00-04:00h, local time) plus mid-morning (11:00-12:00h) deployments using a rosette sampler fitted with 24 water bottles (20L) and a Sea-Bird 9/11 CTD. Standard sampling depths were at the following light levels (as a percent of surface irradiance): 55, 33, 14, 1 and 0.1%. Other samples were taken at selected depths in order to fill- in the profile depending on the shape of the chlorophyll fluorescence profile, especially across the deep chlorophyll maximum (DCM) and to a maximum depth of 500 m. The percent light estimates were based on either the previous day's measurement with a scalar Photosynthetically Active Radiation (PAR) sensor mounted on the CTD or assuming that the DCM sat at the 1% irradiance light depth (Z_{chlmax}). The diffuse attenuation coefficient for PAR (m $^{-1}$) was approximated as 4.6/ Z_{chlmax} and light depths were calculated as the optical depth divided by the diffuse attenuation coefficient. This approach assumed that the diffuse attenuation coefficient was constant over the euphotic zone. Discrete surface samples were also regularly drawn from the ships' underway seawater lines for calibration and validation of the underway sampling system. Nutrient analyses were performed to measure concentrations of nitrate, phosphate and silicate, using a Technicon, five-channel autoanalyser (Bran + Luebbe AAII) (Kirkwood, 1989; Woodward and Rees, 2001). While some nutrient sections have been previously published from individual AMT cruises, the mean nutrient sections (and their variance) presented here, are unique for the group of cruises presented in Table 2 and have heretofore never been published.

2.2. Discrete sample analyses

The technique of Poulton et al. (2006b) was used to measure CaCO₃ concentration (particulate inorganic carbon; PIC). Briefly, 100-200 mL samples were filtered onto 0.4µm pore-size polycarbonate filters and rinsed first with filtered sea water, then potassium tetraborate buffer (adjusted to pH = 8.3) to remove sea water calcium chloride. This pH adjustment was critical to insure that carbonates were stable during sample storage. Later, filters were placed in trace metal-free centrifuge tubes with 5 mL 0.5% Optima grade nitric acid and the Ca concentration measured using inductively-coupled-plasma optical emission spectroscopy (Cheng et al., 2004) which has a precision of \pm 1.9%. Chlorophyll a concentrations were measured using 250mL seawater aliquots filtered through 25mm diameter Whatman GF/F glass fiber filters, extracted in 90% acetone at 4°C for 18-20h (Poulton et al., 2006a) with fluorescence measured using a TD700 Turner Designs fluorometer, calibrated using purified chlorophyll a (Sigma-Aldrich). The precision of this method is $<\pm 10\%$ for replicate measurements. For measuring particulate organic carbon (POC), 1-4.2L of seawater

Specific cruise details (ship, location, number of stations ("Stn") and number surface underway ("UW") samples and dates) for data used in this work. For cruise numbers with asterisks, only results for scanning electron

inicroscopy are being presented in this work.	IIIS WOLK.						
Cruise	Ship	Sampling Domain	# Stn Profiles	# Surf. UW Samples	Date First Stn	Date Last Stn	# Sample Days
Atlantic Meridional Transect 15	RRS Discovery	North and South Atlantic Ocean	63	112	9/19/2004	10/26/2004	38
Atlantic Meridional Transect 16	RRS Discovery	North and South Atlantic Ocean	53	131	5/21/2005	6/26/2005	37
Atlantic Meridional Transect 17	RRS Discovery	North and South Atlantic Ocean	52	175	10/18/2005	11/26/2005	40
Atlantic Meridional Transect 18	RRS James Clark Ross	North and South Atlantic Ocean	51	111	10/4/2008	11/8/2008	36
Atlantic Meridional Transect 19	RRS James Cook	North and South Atlantic Ocean	29	110	10/14/2009	11/27/2009	45
Atlantic Meridional Transect 20	RRS James Cook	North and South Atlantic Ocean	09	134	10/13/2010	11/22/2010	41
Atlantic Meridional Transect 21	RRS Discovery	North and South Atlantic Ocean	89	94	9/30/2011	11/9/2011	41
Atlantic Meridional Transect 22	RRS James Cook	North and South Atlantic Ocean	29	06	10/11/2012	11/20/2012	41
Atlantic Meridional Transect 24*	RRS James Clark Ross	North and South Atlantic Ocean	248	0	9/22/2014	11/2/2014	41
Atlantic Meridional Transect 25*	RRS James Clark Ross	North and South Atlantic Ocean	29	3	9/15/2015	11/3/2015	49
Total			962	096			409

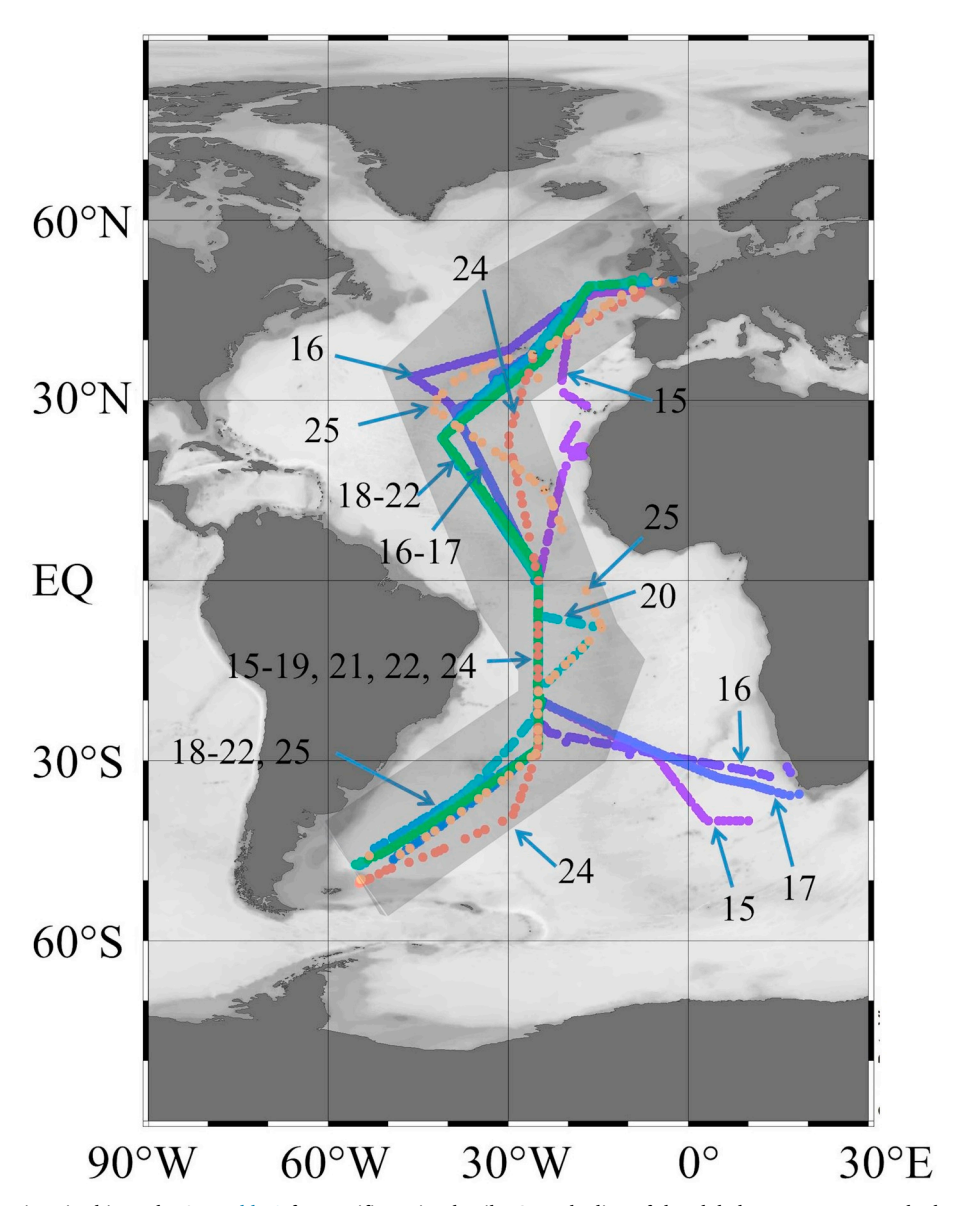


Fig. 1. Map of station locations in this study. See Table 2 for specific cruise details. Gray shading of the global oceans represents bathymetry (darker regions are shallower). Dark grey region surrounding cruise tracks shows the data that are included in the mean sections shown later in this paper. Data outside of this region represent 1.2% of the total data set.

were filtered through pre-baked (> 400° C, 12h) 25mm diameter Whatman GF/F filters and stored at - 20° C. Filters were then acid fumed (to remove PIC) and POC measured using a Thermo Finnegan Flash EA1112 Elemental Analyser (Poulton et al., 2006b). Filters wetted with filtered seawater were used as blanks. The root mean square difference (RSD) of the technique is \pm 10-15%. Biogenic silica was measured using the NaOH digestion technique (Brzezinski and Nelson, 1989) which is based on the original technique of Paasche (1973b). The technique dissolves > 98% of the amorphous (biogenic) silica and < 1% of the mineral silica, after which the reactive silicate was analyzed (Parsons et al., 1984). The RSD of the technique is \pm ~15% (Demarest et al., 2011).

Microscope enumeration of plated coccolithophore cells and coccoliths (for total abundance) were performed using polarized light microscopy, a relatively inexpensive and fast technique for measuring total numbers of coccolithophore cells and detached coccoliths (but providing less reliable species information than SEM). Water samples of $50\text{-}100\,\text{mL}$ were filtered through a 25mm diameter Millipore HA filter, rinsed with potassium tetraborate buffer (pH = 8.3), and frozen in a

petri dish until counted (Haidar and Thierstein, 2001; Haidar et al., 2000). Prior to mounting, the filters were dried in an oven at 60°C. Canada Balsam (60°C) or Norland brand optical adhesive was first placed on top of a cleaned microscope slide, then the sample filter was placed on top of this, followed by a cover slip. The filter was examined with an Olympus BH2 microscope equipped with polarization optics and automated sample stage after which, birefringent coccoliths and plated coccolithophore cells were imaged and enumerated. The filters were counted at a magnification of 400X and 150-200 images were taken of each slide. Given the magnification, volume filtered, and numbers of microscope fields examined, the effective volume counted per sample was 1.69-3.38 mL. Detached coccoliths, plated coccolithophore cells and aggregates of coccoliths were imaged automatically with images processed using CCC image-analysis software (Balch and Utgoff, 2009). Detailed light microscopy of cells, cell walls, organelles, (and absolute species identification) is difficult on HA filters treated with Canada Balsam or Norland-brand optical adhesive using transmitted light, whereas birefringence patterns of coccoliths can still be easily discerned in polarized light. Thus, when presenting birefringence

microscopy results for coccolithophore cells, we combine counts of plated cells and coccolith aggregates as coccolithophores since it is difficult to discriminate between the two categories, in practice. For this reason, it is not possible to cross-calibrate species identification between the birefringence counts and the SEM counts (below). Nonetheless, as there is considerable birefringent debris in ocean water, polarization microscopy is still a highly reliable way to discriminate birefringent debris from coccoliths (Balch and Fabry, 2008) (as the latter have distinct birefringence patterns that can aid in identification (Moshkovitz and Osmond, 1989)). All water column integration of the above variables used standard trapezoidal integration.

Scanning electron microscopy was only performed on AMT cruises 24 and 25 (Table 2). All but seven samples were taken from the surface and DCM. Samples were prepared for SEM analysis by filtering 100mL seawater onto a 0.4µm pore-size, 25mm diameter, polycarbonate filter, rinsing with potassium tetraborate buffer, then drying the filter at 60°C. The effective filter area of the polycarbonate filter had a diameter of 21mm. Filters were cut and mounted on aluminum SEM stubs (12.7mm diameter) and gold coated prior to analysis on Bigelow's Zeiss Supra25 field emission SEM, according to Goldstein et al. (2003). Typically, filters were examined at 15,000X magnification (field diameter = 240µm) across the entire stub length of 12.7mm (with a range of 8,000X to 42,000X for imaging, depending on the size of the coccolith or coccolithophore cell). The effective volume of sample thus examined was 0.88 mL. The identification of coccolithophore species was done according to Young et al. (2003). All taxa with full citations are given at the Nannotax website (http://mikrotax.org/Nannotax3). A list of the species encountered during AMT 24 and 25 is given in the Supporting Information (Table S1) and included 110 species. For AMT 25, in addition to the enumeration of all the coccolithophore species, we also classified three observed morphotypes of Emiliania huxleyi, Types A, B and C (Poulton et al., 2011). Diversity (H'), richness (S) and evenness (J') of the assemblages were calculated (Magurran, 2004) for both the coccolithophore cells as well as the detached coccoliths (for which species origin could be determined).

2.3. Data analysis

There was no standard ship track for the AMT cruises (Fig. 1), therefore we report the mean sections of each variable, plotted against latitude using Ocean Data View (ODV; Version 5) (Schlitzer, 2018). Since all but three of the cruises ended in South America, the mean section used in this analysis was centered on the South American cruise track (Fig. 1; see shaded area). Data from east of 15°W in the South Atlantic (on the opposite side of the Atlantic basin; AMT 15-17) were, thus, not included in the mean section. The data near the coastal Mauritanian upwelling (AMT15 only) were also not included in the mean section as they were in the highly eutrophic, West African upwelling system. These data (57 of 4,579 samples) represented only $\sim 1.2\%$ of the entire data set. Inter-cruise variance of coccolithophore concentration, biogeochemical and nutrient results were calculated for cruises 15-22 using Ocean Data View. Data were gridded in the horizontal at 10° latitude increments (\pm 5° latitude) and depth binning of $10(\pm 10)$ m, $30(\pm 10)$ m, $50(\pm 10)$ m, $70(\pm 10)$ m, $90(\pm 10)$ m, $125(\pm 25)$ m, $200(\pm 50)$ m, $300(\pm 50)$ m, and $500(\pm 150)$ m. Variance was described using the coefficient of variation (CV = standard

As noted earlier, all AMT cruises except one (AMT16), took place in the northern hemisphere fall/southern hemisphere spring. AMT16 took place in the southern hemisphere austral fall/northern hemisphere spring. In order to determine whether we could group AMT16 data with the rest of the AMT cruises in our analysis, we tested whether cruise sections for each variable (as a function of latitude and depth) were significantly different for AMT16 versus all other cruises. We performed a Model II ANOVA, two-factor analysis, examining the least-square-fit relationship between each variable in question (e.g. chlorophyll,

coccolithophore abundance, etc.) as a function of both latitude and depth. For all variables except temperature, salinity and oxygen, data were log transformed first as they were log-normally distributed (Campbell, 1995). We compared the cruise groups in two ways: 1) we examined the significance of the least-square relationship for each variable as a function of latitude and depth (using the F statistic with the associated model and error degrees of freedom) and then 2) we tested if the means for model predictions for the two cruise groups were significantly different from each other based on their RMSE. The results are given in Table S1 (Supporting Information); they show that each variable could be modeled as a statistically-significant relationship (P < 0.01), in fact most showed P < 0.001) as a function of latitude and depth for the cruise compilations that included all cruises except AMT 16 (the number of data points ranged from 1332 to 6600). For AMT16 data alone, all variables could also be significantly modeled (P < 0.01) as a function of latitude and depth, except for log₁₀ PIC and log₁₀ chlorophyll. Based on the sectional data, and associated RMSE errors in measurements, the mean predicted variables between cruise groups were not statistically different from each other for any of the variables (p < 0.05) (Table S1) and grouping all the AMT cruises into a single group is justified.

3. Results

3.1. Vertical sections of biogeochemical variables and coccolithophore/coccolith concentration

The section of PIC concentration along the North and South Atlantic showed highest concentrations (0.25 μM) within the north temperate waters (NTW) and south temperate waters (STW) (roughly within the top 250-300m depth) (Fig. 2A). Moreover, there was a surface and deep PIC maximum at 300m (0.1-0.15µM) in the North Subtropical Gyre (hereafter, referred to as the North Atlantic Gyre, NAG), Equatorial region (EO) and STW. The water mass definitions that we use in this work were given elsewhere (Robinson et al., 2006a). A distinct surface minimum in PIC concentration ($\sim 0.06 \,\mu\text{M}$) was found in the upper 50m of the EQ and in the NAG near the 27 sigma theta density anomaly (σ_{θ}) isopycnal at ~200m. The very lowest PIC concentrations (< 0.04µM), however, were observed at 500m of depth in the south subtropical gyre hereafter referred to as the South Atlantic Gyre (SAG; measured on eight different occasions from three different cruises, AMT17, 21 and 22). Note that the SAG was the only region where such deep samples were taken. The mean section of POC concentration showed greatest values in the top 100m of the entire section, above the σ_{θ} of 27 (Fig. 2B). Highest concentrations of POC (10-16 μ M) were observed in the top 100m of the STW, with lower values (3-4 μ M) observed in deep waters of the SAG, EQ and NAG. The mean section of BSi concentration showed maximum concentrations of 0.3µM in the STW, with subsurface maxima ($\sim 0.03 \mu M$) in both the SAG and NAG between 100-200m (26-27 σ_0 ; in the region of the DCM; Fig. 2C and D), slightly deeper in the SAG. In contrast to the SAG and NAG, there were typically more vertically uniform BSi concentrations in the NTW and EQ waters (0.03-0.05µM) and STW waters (0.2-0.3µM), at least down to 300m depth (Fig. 2C). Maximum concentrations of chlorophyll were 1-2µg L⁻¹ seen in the STW. There was a pronounced DCM with concentrations of $0.5 \mu g L^{-1}$, the DCM was found between the σ_{θ} of 27 isopycnal (deepest) and 26 σ_{θ} isopycnal (shallowest), except in the NTW where it extended upwards to σ_{θ} 25.5 and the EQ region where it outcropped at the sur-

Concentrations of coccolithophore cells showed a dynamic range of almost an order of magnitude, with peak abundance in the upper depths of the NTW and STW (100-200 cells mL⁻¹; Fig. 2E). Both the NAG and SAG showed highest concentrations in the upper 100m (50-60 cells mL⁻¹), higher than surface concentrations in the EQ (typically 40-50 cells mL⁻¹). There were deep coccolithophore populations at 20°S in the SAG, down to 200m depth. The concentration of coccolithophore cells

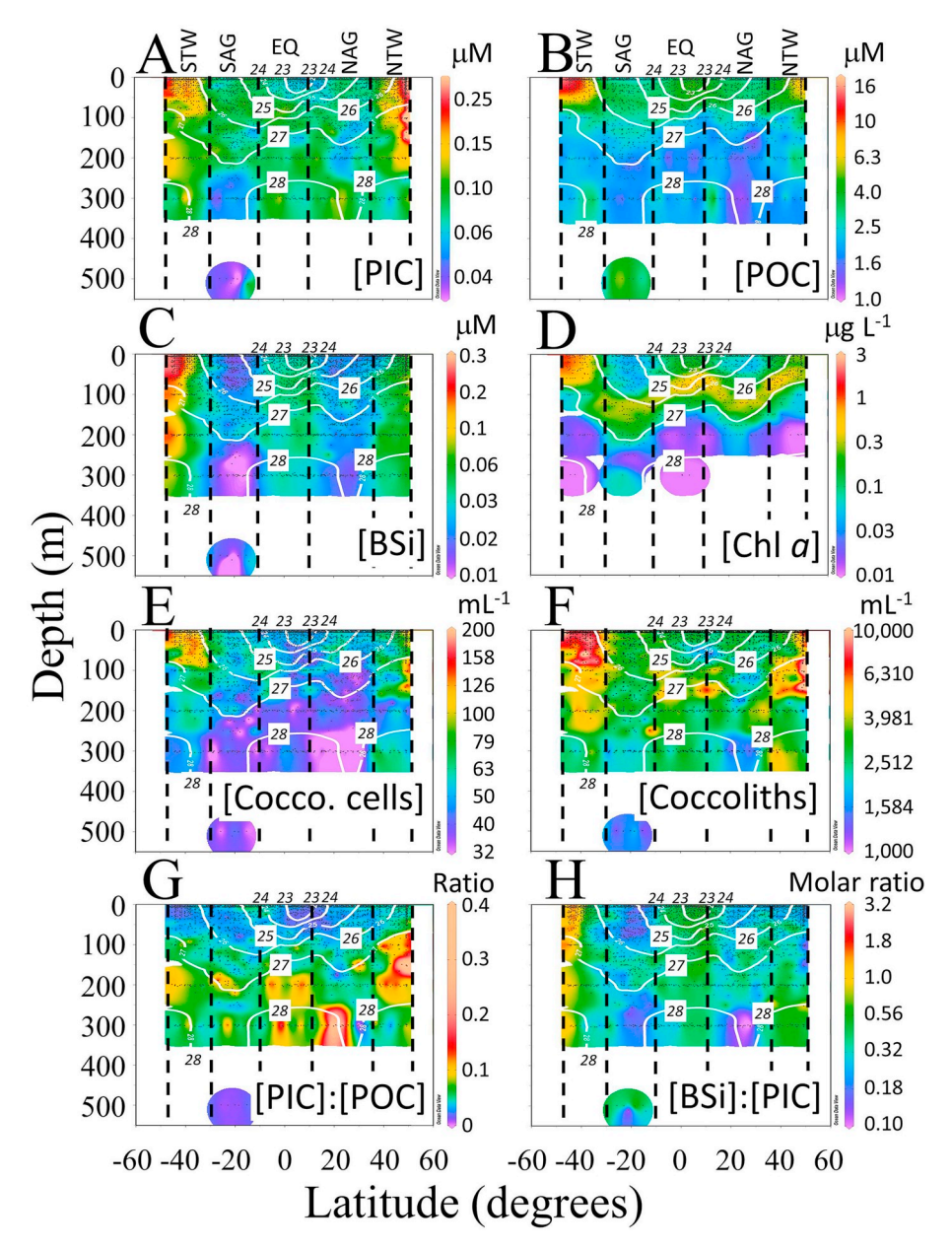


Fig. 2. North-South mean sections along AMT transects (showing sections that end in South America) of concentration of (A) PIC (μ M), (B) POC (μ M), (C) BSi (μ M), (D) chlorophyll a, (μ g L⁻¹), (E) coccolithophore cells (μ L⁻¹), (F) detached coccoliths (μ L⁻¹), (G) PIC:POC ratios, and (H) BSi:PIC molar ratios. Isopleths of density anomaly (σ ₀) are shown in white. Regional water masses designated across the top of panels A and B, and demarcated in all panels with vertical dashed lines.

decreased dramatically below the NAG and SAG, with mean values of $\sim 30 \text{mL}^{-1}$ below 250-300m of depth. Deep concentrations of coccolithophores were greatest (60 cells mL⁻¹) in the NTW ($\sim 50^{\circ}\text{N}$, $\sim 300 \text{m}$) and STW (south of 30°S, ~ 200 -250m; Fig. 2E).

The concentration of detached coccoliths varied over about one order of magnitude from $1000\text{-}10,000\,\text{mL}^{-1}$ (Fig. 2F). Highest coccolith concentrations ($\sim 10,000\,\text{mL}^{-1}$) were observed at the poleward extremes of the transect in the top 100-150m. Coccolith concentrations were $2,500\,\text{mL}^{-1}$ in both the NAG and SAG and the distributions showed relative patterns similar to the coccolithophore cells described above. Regions with lowest detached coccolith concentrations (1,000-1,600 coccoliths/mL) were observed below 300m depth in the NAG and 500m depth in the SAG. However the SAG was the only region where 500m samples were taken, thus we cannot infer the NAG had similarly low values at 500m. There were subsurface maxima in coccolith concentration ($6000\text{-}7000\,\text{mL}^{-1}$) on north and south extremes of the EQ, centered in waters with densities between σ_0 26-27.2. There were also

subsurface peaks in coccolith abundance (2000-3000mL⁻¹) between σ_{θ} 27 and 27.5 in both the NAG and NTW. There were elevated concentrations of detached coccoliths ($\sim 2000\,\text{mL}^{\text{-}1})$ at 300-350m in the STW, EQ and NTW regions (Fig. 2F).

The PIC:POC ratio varied between 0 to ~ 0.4 over the transect with generally increasing values with increasing depth (beginning at a $\sigma_{\theta} \sim 26.5$ - 27; Fig. 2G). This was true, even in the SAG and south EQ waters, where there were slightly elevated PIC:POC ratios in the top 20m depth but values still increased with depth. The highest PIC:POC ratios (> 0.2) were found in the NAG and NTW at 100-300m depth. For the very deepest samples in the SAG (500m), PIC:POC ratios declined to values close to zero, as PIC approached zero (Fig. 2A).

The ratio of BSi:PIC showed highest values of 1-2 in the southern part of the STW from 0-300m depth. The subtropical gyres (NAG and SAG) generally showed lowest values of the BSi:PIC ratio overall (0.1-0.2) with values of 0.3-0.5 in the depth of the DCM (Fig. 2D, H). BSi:PIC ratios < 1 were observed over the remainder of the study area with a

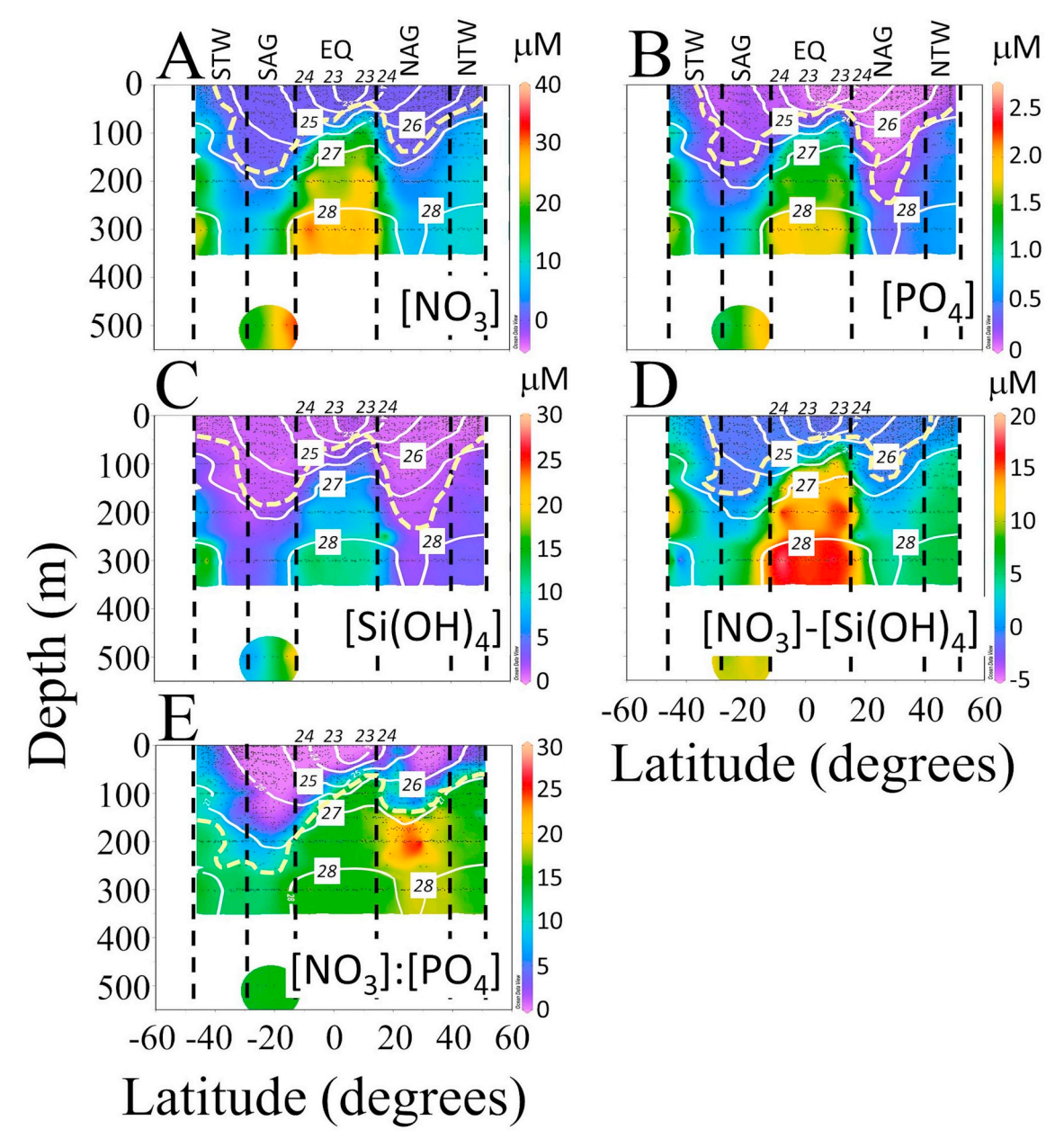


Fig. 3. North-South combined sections along AMT transects (showing data for transects that end in South America) for (A) nitrate (μ M; canary-colored dashed contour designates the 1 μ M nitracline) (B) phosphate (μ M; canary-colored dashed contour designates the 0.2 μ M nitracline), (C) silicate (μ M; canary-colored dashed contour designates the 1 μ M silicicline), (D) nitrate-silicate (residual nitrate; μ M; canary-colored dashed contour designates the 0 μ M residual nitrate contour), and (E) nitrate/phosphate molar ratio (canary-colored dashed contour designates the Redfield Ratio of 16). Isopleths of density anomaly (σ ₀) are shown in white. Regional water masses designated across the top of panels A and B, and demarcated in all panels with vertical dashed lines.

clear region of ratios of 0.5 under the EQ zone.

The average distributions of nitrate, phosphate and silicate are shown as north-south mean sections with water density overlaid (Fig. 3). The nutrient sections generally showed asymmetry between the NAG and the SAG with nutrient drawdown occurring at different depths in the SAG and NAG. Nutrient concentrations showed some concurrence with the density field but the nutriclines were not always associated with the same isopycnal. The nitracline (defined as the depth where the nitrate concentration was 1µM) was between the σ_{θ} of 26 and 27 in the STW and NTW, closer to the σ_{θ} 27 isopycnal in the SAG and NAG and shallower than the σ_{θ} 25 isopycnal in the EQ waters (Fig. 3A; see canary-colored dashed line). The depth of the phosphate nutricline (here defined as the depth where phosphate was 0.2µM) was similar to the nitracline in the STW, SAG, EQ and NTW but in the NAG, the phosphate nutricline was between 200-300m depth (Fig. 3B), well

deeper than the nitracline. The relative distribution of silicate was similar to the phosphacline, with roughly similar depths of the silicate nutricline (here defined as the depth where silicate concentration was 1 μ M; Fig. 3C). The difference between nitrate and silicate concentrations ("residual nitrate" (Barrett et al., 2018; Sarmiento et al., 2004; Townsend et al., 2010)), had positive values over the entire water column in most of the STW. In the SAG, NAG and NTW, residual nitrate was negative shallower than the 26.5 σ_{θ} isopycnal while in the EQ, there were negative residual nitrate values above the 24 σ_{θ} isopycnal (Fig. 3D). The ratio of nitrate to phosphate fell below the Redfield Ratio (molar ratio of 16 (Redfield et al., 1963)) shallower than the: (a) 27.5 σ_{θ} isopycnal in the STW and SAG, (b) 25-27 σ_{θ} isopycnals in the EQ and (c) 26-27 σ_{θ} isopycnals in the NAG and NTW.

PIC concentration showed a high overall intercruise CV (0.6-4.4; meaning that the standard deviation was \pm 60-440% of the mean).

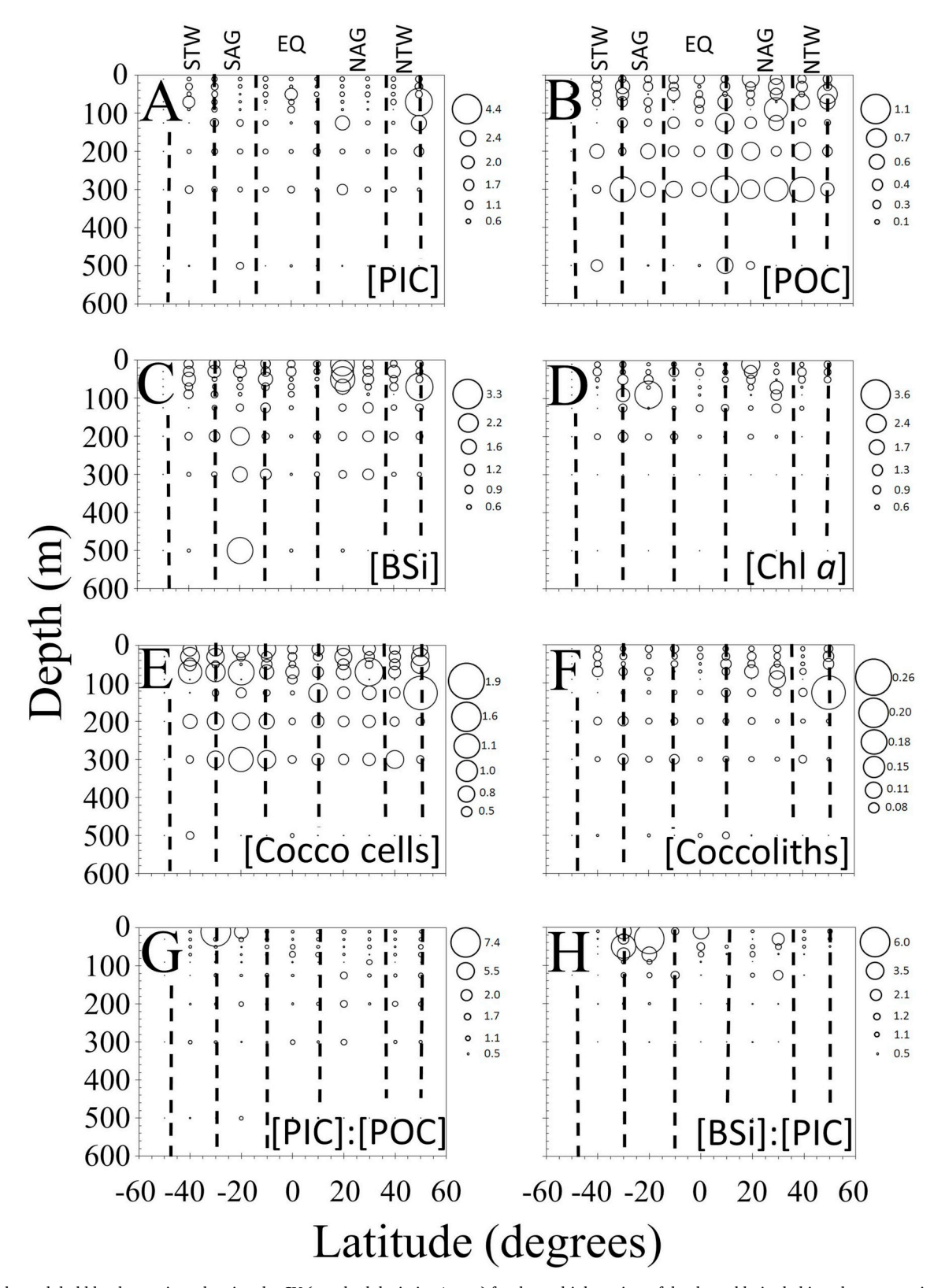


Fig. 4. North-south bubble-plot sections showing the CV (standard deviation/mean) for the multiple cruises of depth- and latitude-binned concentrations of (A) PIC (μ M), (B) POC (μ M), (C) BSi (μ M), (D) chlorophyll a (μ g L⁻¹), (E) coccolithophore cells (μ L⁻¹), (F) detached coccoliths (μ L⁻¹), (G) PIC:POC ratios, and (H) BSi:PIC molar ratios. Bubble size key shown to the right of each panel. Smallest dots indicate depths with no data.

Highest PIC CV values of 2-4 were observed in the NTW at depths shallower than 125m (Fig. 4A) as well as in the NAG between 125-300m (CVs of 0.6-2). The only other regions showing elevated PIC CVs were in the top 100m of the EQ and STW. The remaining waters showed

PIC CV values of 0.6-1 (Fig. 4A). CV values for POC ranged from 0.1-1.1 and the greatest CV values were generally seen at 300m depth and it was patchy at shallower depths (Fig. 4B). BSi CVs ranged from 0.6-3.3 over all the AMT cruises, with peak values in the NTW and NAG (upper

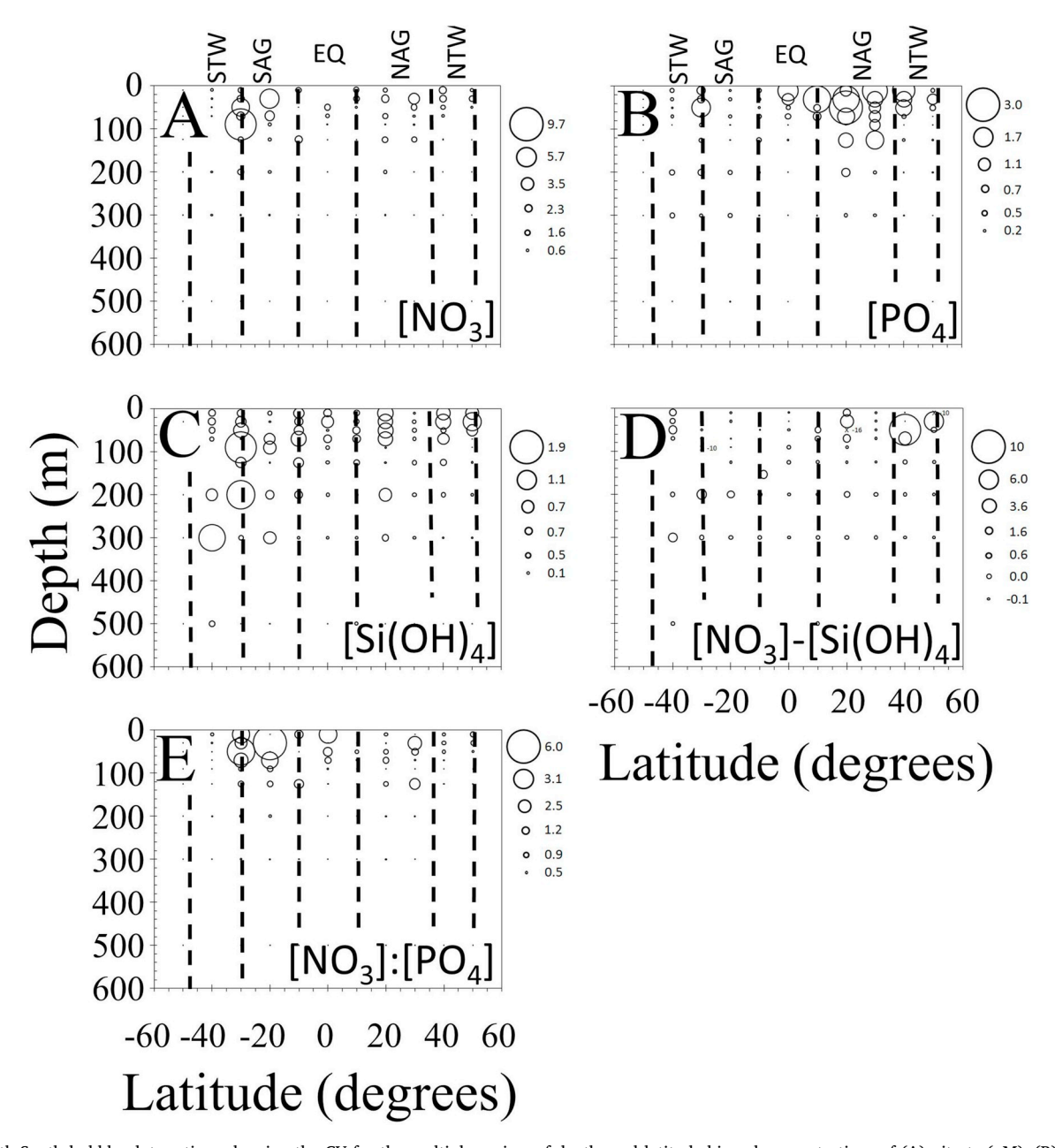


Fig. 5. North-South bubble-plot sections showing the CV for the multiple cruises of depth- and latitude-binned concentrations of (A) nitrate (μ M), (B) phosphate (μ M), (C) silicate (μ M), (D) nitrate-silicate (residual nitrate; μ M), and (E) nitrate/phosphate molar ratio. Bubble size key shown to the right of each panel. Smallest dots indicate depths with no data.

125m) and deeper depths of the SAG (200-500m) (Fig. 4C). Chlorophyll a was only sampled in the euphotic zone and showed CVs ranging from 0.6-3.6, overall. Highest CVs for chlorophyll a were found in the NAG and SAG (upper 100m) (Fig. 4D). The inter-cruise variance in the concentration of coccolithophore cells showed CV values of 0.5-1.9 (Fig. 4E). CV values for coccolithophore cell concentrations were generally highest in the top 125m of the water column. The SAG showed higher coccolithophore CVs down to 300m depth (Fig. 4E). Relative to the coccolithophore cells, the concentrations of detached coccoliths demonstrated far lower inter-cruise variability with CVs ranging from 0.08-0.26. Except for the 125m depth in the NTW, typical CVs of the concentration of detached coccoliths were < 0.1. The PIC:POC ratio showed two locations near the surface in the SAG and STW with CV of > 2, otherwise the PIC:POC ratio had a CV of < 1 (Fig. 4G). The BSi:PIC ratio showed greatest inter-cruise variance (CV up to 6) in the top 100m of the SAG, STW and in the EQ. Otherwise, the CV of the BSi:PIC ratio typically was < 1.

The variability of the nutrients between cruises was significant (Fig. 5) and there was greater overall variability for nitrate than for phosphate or silicate. For example, the CV of nitrate was 0.6-9.7 with the highest values (by far) observed in the SAG and its border with the STW. Otherwise, nitrate CV values were 0.6-2.3 with slightly higher values of 2-3 in the surface NAG (Fig. 5A). Cruise variability in phosphate showed CVs from 0.2-3, with a trend slightly different from nitrate with the greatest phosphate CVs observed in the NAG, EQ and border with the NTW (Fig. 5B) and some moderately elevated values at the border between the STW and SAG. Silicate CVs had overall variability of 0.1-1.9, with highest values generally in the top 125m. However the largest silicate CV was observed in the top 300m in the STW and SAG (Fig. 5C). Residual nitrate CVs varied overall between 0.1 and 10 with greatest inter-cruise variance in the upper 100m of the NTW and its border with the NAG (Fig. 5D). The nitrate:phosphate ratio CV ranged between 0.5 and 6 with greatest inter cruise variance in the SAG and its border region with the STW, above 100m depth.

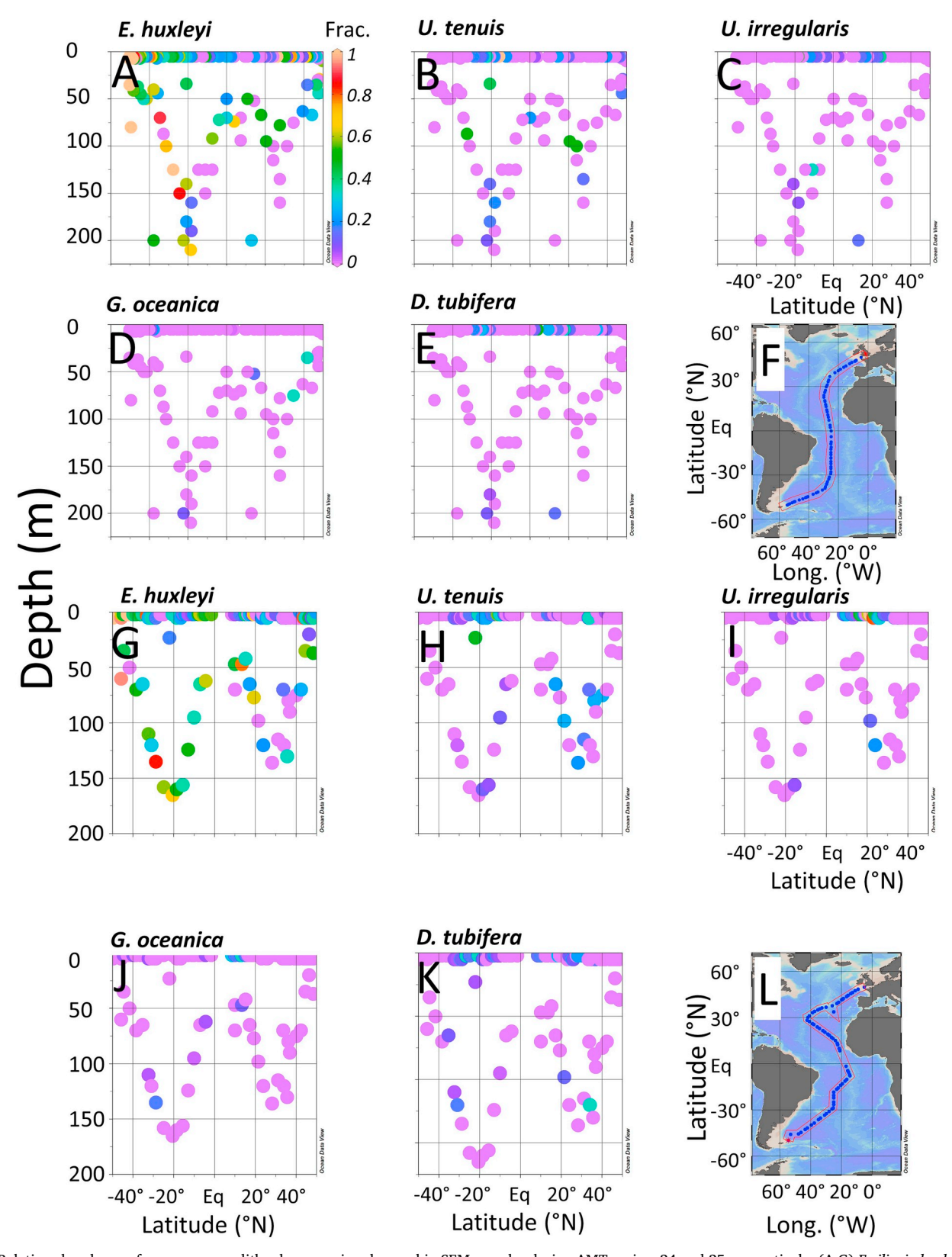


Fig. 6. Relative abundance of common coccolithophore species observed in SEM samples during AMT cruises 24 and 25, respectively: (A,G) *Emiliania huxleyi*, (B,H) *Umbellosphaera tenuis*, (C,I) *Umbellosphaera irregularis*, (D,J) *Gephyrocapsa oceanica*, and (E,K) *Discosphaera tubifera*. (F,L) Cruise tracks of AMT 24 and 25 shown for reference.

3.2. Scanning electron microscopy results

Using SEM, we identified 107 coccolithophore species (Table S2). The coccolithophore species that contributed the largest fraction of the $\frac{1}{2}$

total coccolithophore assemblage for AMT 24 and 25 was *E. huxleyi*. It dominated in both high latitudes of both hemispheres, in both surface and DCM waters (Fig. 6A, G). It generally showed highest fractions of the total floral assemblage in the top 10m (Table S2). Counts of *E.*

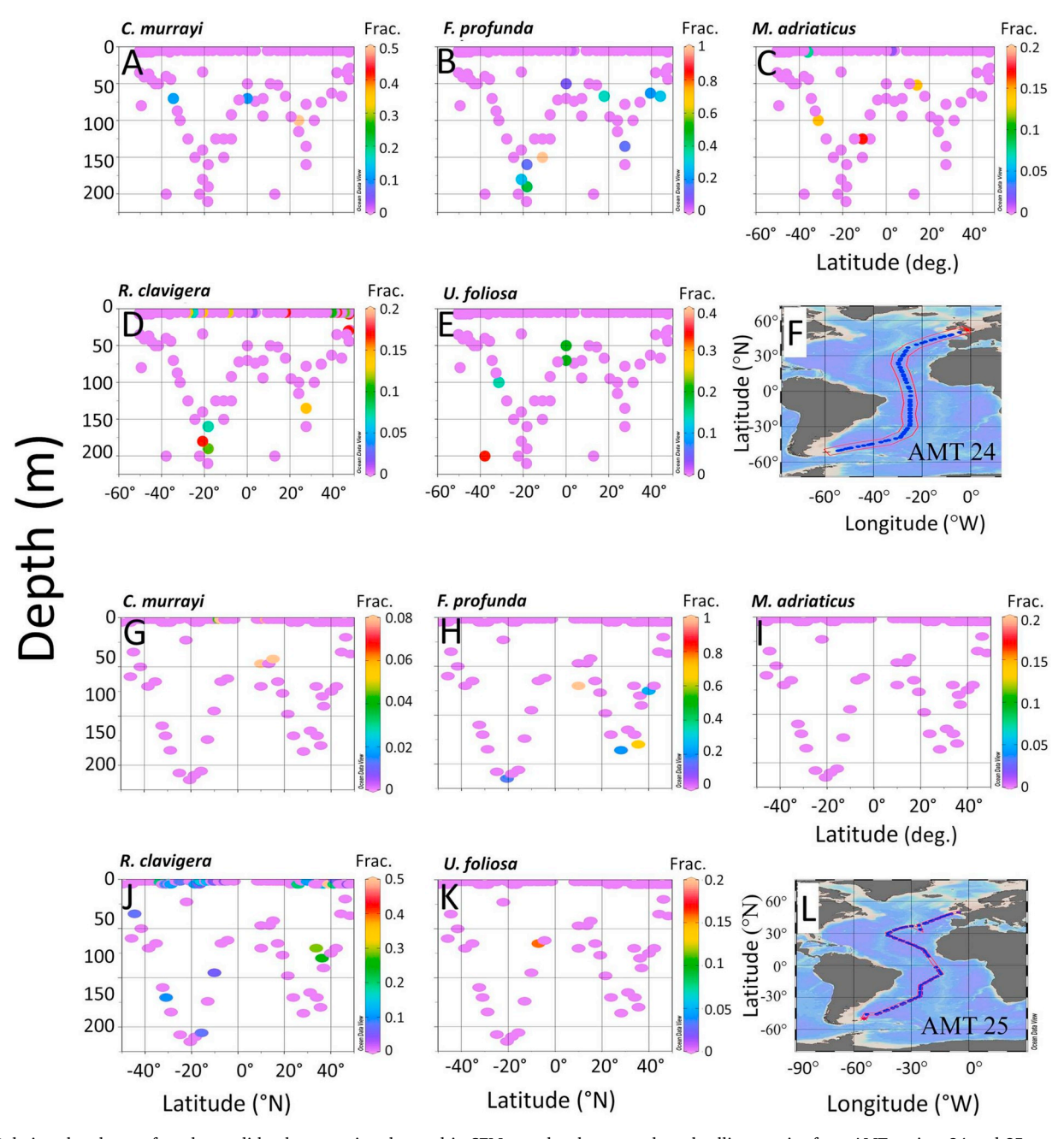


Fig. 7. Relative abundance of total coccolithophore species observed in SEM samples that were deep-dwelling species from AMT cruises 24 and 25, respectively: (A,G) Calciosolenia murrayi, (B,H) Florisphaera profunda, (C,I) Michaelsarsia adriaticus, (D,J) Rhabdosphaera clavigera, and (E,K) Umbilicosphaera foliosa. (F,L) Cruise tracks of AMT 24 and 25 shown for reference.

huxleyi coccospheres and coccoliths from AMT25 were split into three observed morphotypes (Type A, B and C based on the description of Young et al. (2003)) and their fractional abundance of the entire assemblage calculated (Fig. S6). The Type A morphotype of *E. huxleyi* was the most commonly observed at all latitudes, for both coccospheres and detached coccoliths, in surface and deep samples alike (Figs. S6A and D). The Type B morphotype showed lower relative abundances than Type A, contributing, at most, 30-50% of the entire coccolithophore or coccolith assemblages. It was mostly present in the southern hemisphere (Figs. S6B and E). The Type C morphotype of *E. huxleyi* was most abundant at the Subantarctic Front, representing ~30-80% of the respective floral assemblages of coccolithophores and coccoliths (Figs. S6C and F). North of the Subantarctic Front, the relative proportion of Type C *E. huxleyi* was highest in the DCM (Fig. S6C).

A common coccolithophore species was Umbellosphaera tenuis,

predominantly seen in subtropical waters of both hemispheres, more abundant at the surface and less in the DCM (Fig. 6B and H; Table S2). After *E. huxleyi, Umbellosphaera irregularis* was the next most abundant species across the cruises, particularly in surface waters of the tropics (Fig. 6C, I; Table S2). *Gephyrocapsa oceanica* was observed at lower frequencies still and was relatively cosmopolitan but patchily distributed, seen both in surface and mid-depth samples of the tropics and subtropics (Fig. 6D and J; Table S2). *Discosphaera tubifera*, while seen in only a few cases in DCM waters, was more commonly seen in surface samples of the subtropics (Fig. 6E, K; Table S2).

We also examined several coccolithophore species commonly found in the deeper populations (Fig. 7; Table S2). We include a focus on these species since these calcifiers are likely to be important players in the carbonate production within these deep waters, which include the northward-flowing SAMW. These species include: *Calciosolenia murrayi*

Deep-Sea Research Part I 151 (2019) 103066

(which was usually found at 40-100m but we note that it was also observed in several surface SAG and EQ samples during AMT 25 (Fig. 7A and G)), Florisphaera profunda (observed at 50-200m; Fig. 7B,H), Michaelsarsia adriaticus (sampled in two surface samples during AMT 24, otherwise seen between 50-130m with no cells seen in AMT25 counts; Fig. 7C,I), Rhabdosphaera clavigera (seen in a number of surface samples and otherwise observed between 40-200m; Fig. 7D, J) and Umbellosphaera foliosa (observed at 50-200m; Fig. 7E,K).

Diversity (based on the Shannon index; H'), species richness (S) and evenness of the coccolithophore assemblage (J') were calculated for both AMT cruises where SEM data were available. For the two AMT cruises, the ecological indices were compared between the coccolithophore species (based on SEM observations of plated cells; Fig. 8A-C; G-I) versus the species associated with detached coccoliths (Table 3; Fig. 8D-F, J-L). Our results showed that the diversity of the coccolithophores (Fig. 8A,G) was significantly higher than the diversity of species detaching their coccoliths (Fig. 8D, J; Table 3). Species richness was also greater for the plated coccolithophore cells (Fig. 8B,H) than for the species that detached their coccoliths (compare Fig. 8E, K). For AMT24, the evenness of the species that dropped their coccoliths (Fig. 8F) was significantly higher than the evenness of the total coccolithophore assemblage in AMT24 (Fig. 8C) but this was not the case for AMT25 (Fig. 8I,L; Table 3). In summary, the diversity, H', was about double, and S was more than double, for the total coccolithophore species assemblage (107 species) than the coccolithophore species that drop their coccoliths (31 species; Table S2).

We also examined the variability of the ecological indices as a function of absolute value of the latitude (where latitude would incorporate the effects of both the temperature and/or light, for example). All such relationships had low coefficients of correlation. We provide the least-squares-derived relationships in Table 4, only when statistically significant. For AMT24, there was a statistically-significant inverse relationship between H', S and J' plotted against the absolute value of latitude (Figs. S1, S2, S3). For AMT25 there were no significant relationships between H', S or J' when plotted against the absolute value of latitude. However, with removal of a single outlier datum for the AMT25 species richness, the negative relationship indeed became significant (Table 4; Fig. S4). That same sample also had an anomalously high H' but with removal of that datum, the relationship of H' with the absolute value of latitude was still insignificant (P > 0.05; results not shown). A comparison between the ecological indices for the surface and DCM populations showed significant differences for AMT24 (H' and S) and AMT25 (J') (Table 5). In all other cases, the ecological indices were not significantly different between surface and deep assemblages (Table 5; Fig. 8).

The SEM-derived species assemblages were grouped into fractions of placolith-bearing, umbelliform, or floriform coccolithophores as well as a miscellaneous group defined by Young (1994). The miscellaneous group included species that rarely dominate the coccolithophore species assemblage but make up > 80% of the total observed species and < 20% of the total coccolithophore cells. They include families from Helicosphaeraceae, Syracosphaeraceae, Calyptrosphaeraceae (holococcolith bearing species), Pontosphaeraceae and Rhabdosphaeraceae. Placolith-bearing cells represented the largest fraction of surface and deep coccolithophore assemblages in the South Atlantic (STW to the EQ water regions) (Fig. 9A, F). Umbelliform coccolithophores were mainly observed in the subtropical gyres (surface and fluorescence maximum depths) (Fig. 9 B,G). With few exceptions (e.g. AMT24), the floriform species were confined to the fluorescence maximum depths) (Fig. 9 C,H). It should be noted that the fraction of species not included in these first three groupings, was, at times, over half of the observed species, more so in AMT 24 than in AMT25 (Fig. 9D, I).

3.3. Biological and biogeochemical variability as a function of water masses and chemistry

In order to understand the biological and biogeochemical variability associated with water masses along the upper 500m of the AMT transect, a number of the variables from each cruise were plotted in temperature/salinity space (Fig. 10), Lowest density waters were found in shallow waters of the EQ (Fig. 10A and B) while, generally, the densest waters in the upper 500m generally fell between the 26.5 and $27 \sigma_{\theta}$ isopycnals, extending from the southern hemisphere into the northern hemisphere (Fig. 10B). The density isopycnals of SAMW are marked with coarse dashed lines (shallow limit) and fine dashed lines (deeper limit) in the T/S plots of Fig. 10). SAMW is formed between the Polar Front and Subantarctic Front (Cerovečki et al., 2013). During the AMT cruises, SAMW was characterized by the ratio of dissolved inorganic nitrogen to dissolved inorganic phosphorus (DIN/DIP) molar ratios near the Redfield Ratio of 16 (Fig. 10C) and residual nitrate values of 5-15µM, indicating a general excess of nitrate over silicate (Fig. 10D). Highest coccolithophore cell concentrations were found in shallower waters above the SAMW, at 30°S-40°S (Fig. 10E), with low DIN/DIP ratios (of 0-3) and residual nitrate values near zero (Fig. 10D). Highest BSi concentrations were seen within the SAMW and just above it (Fig. 10F). Elevated PIC concentrations were observed in the same shallow water mass that contained the highest coccolithophore concentrations. Moreover, high PIC concentrations were also observed at 200m depth within the SAMW (Fig. 10G), which also corresponded to waters with PIC:POC ratios of ~ 0.1 or higher (Fig. 10H).

In order to examine the same variables, but as a function of nutrient chemistry, we plotted them as a function of silicate and phosphate concentrations (as log-log plots; Fig. 11). Silicate was chosen due to its strong obvious relevance to diatoms while phosphate was chosen due to its strong relevance to coccolithophore growth (Thierstein et al., 2004; Townsend et al., 1994). Log-log plots helped elucidate the variability at low nutrient concentrations. Moderate-to-high coccolithophore cell concentrations were observed when silicate concentrations were ~ 0.1 -2μM and phosphate concentrations were 0.08-1μM (Fig. 11E). A polygon was drawn by eye around these data points in Fig. 11E containing the highest coccolithophore concentrations, and that polygon was reproduced in Fig. 11A-D, F, G to examine associated biogeochemical variability within these low nutrient waters with elevated coccolithophore concentrations. For example, elevated concentrations of coccolithophores were observed at depths of 0-150m (Fig. 11A), σ_{θ} isopycnals of 26-27 (Fig. 11B), DIN/DIP molar ratios less than the Redfield Ratio (Fig. 11C), residual nitrate concentrations of 0 to slightly positive values (Fig. 11 D), moderate-to-high BSi concentrations (Fig. 11F), moderate-to-high PIC concentrations (Fig. 11G) and a high range of PIC/POC ratios (Fig. 11H).

3.4. Relating particle abundance to biogeochemical variables

The concentration of detached coccoliths was significantly correlated to the total concentration of coccolithophore cells over all cruises (Fig. 12, note the log axes). The least-squares fit power function to these results is given in the figure legend. The significance of this relationship is that at low concentrations of coccolithophores, the ratio of detached coccoliths to plated coccolithophore cells averages ~40 while at elevated concentrations, the ratio of detached coccoliths to plated coccolithophore cells is ~ 90 . The concentration of PIC was highest (3 µmol L⁻ 1) in stations with greatest concentrations of coccoliths and plated cells (Fig. 12). The euphotic zone concentration of coccoliths was also examined as a function of the POC:chlorophyll ratio (Fig. 13). Highest euphotic integrated coccolith concentrations (1 x1010 to 3x1010 coccolithophores m⁻²) were typically associated with waters containing integrated POC:Chl ratios > 360 (by mass), where integrated chlorophyll concentrations were < 15mg m⁻², characteristic of more oligotrophic environments.

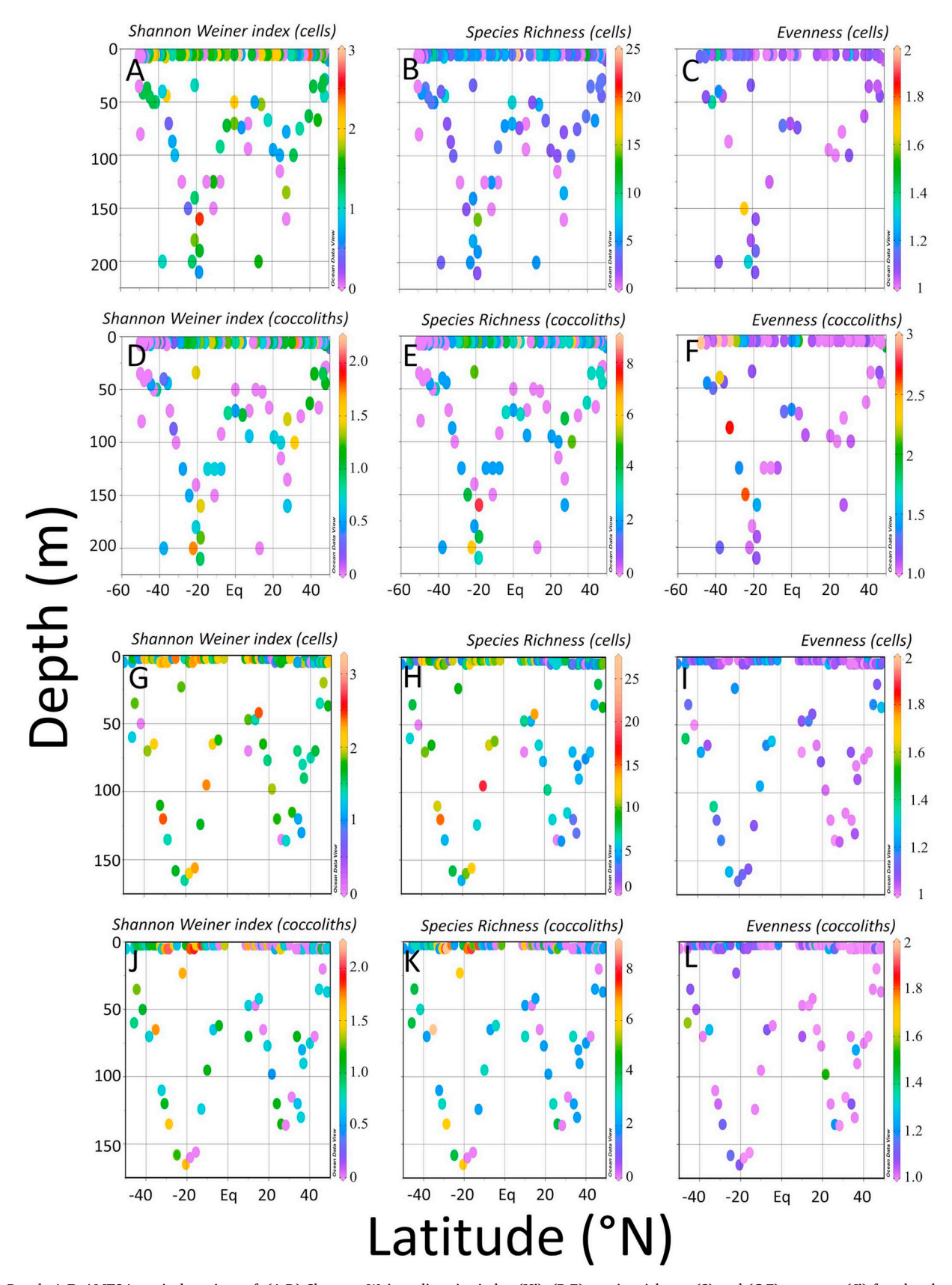


Fig. 8. Panels A-F: AMT24 vertical sections of: (A,D) Shannon Weiner diversity index (H'), (B,E) species richness (S) and (C,F) evenness (J') for plated cells and coccoliths, respectively. Cruise track for AMT 24 can be found in Fig. 1. Panels G-L: AMT25 vertical sections of (G,J) Shannon Weiner diversity index (H'), (H,K) species richness (S) and (I,L) evenness (J') for plated cells and coccoliths, respectively. Cruise track for AMT 25 can be found in Fig. 1.

Table 3
Statistics for mean diversity (H'), species richness (S) and evenness (J') for coccolithophores and detached coccoliths for AMT24 and AMT25. Statistically different averages (alpha level < 0.05) are also designated with bold face font.

Index	Cruise	Mean coccolithophores	Mean coccoliths	DF	t Stat	t crit (2-tailed)	P <
H'	AMT24	1.091	0.521	229	7.418	1.970	2.30E-12
	AMT25	1.628	0.754	208	11.137	1.971	6.75E-23
S	AMT24	4.073	1.831	184	6.140	1.973	4.98E-09
	AMT25	7.162	2.562	163	10.138	1.975	4.92E-19
J'	AMT24	1.099	1.387	66	-2.950	1.997	4.39E-03
	AMT25	1.121	1.090	141	1.783	1.977	7.68E-02

4. Discussion

4.1. Vertical distributions of coccolithophores: are there typical patterns?

The vertical distributions of coccolithophore cells observed in these AMT cruises, especially in the NAG and SAG, showed that by 150-200m, the concentrations decreased to about one third of the surface values (Fig. 2E). Moreover, the concentrations of detached coccoliths decreased to 10% of surface values below the NAG and SAG at depths of 300-400m (Fig. 2F). This is consistent with previous observations although there are relatively few vertical profiles of coccolithophore cells published elsewhere with the latitudinal range described here (Honjo and Okada, 1974; Okada and Honjo, 1973b; Poulton et al., 2017). Hagino et al. (2000) observed that in stratified waters, highest abundance of coccolithophore cells was observed at the thermocline, and decreasing below this depth. In more mixed conditions, coccolithophore cells were biased to the upper euphotic zone (Balch et al., 2018). Oligotrophic waters at the Bermuda Atlantic Time Series have suggested strong subsurface maxima of haptophytes (either as haptophyte pigments or cell counts) centered between 60-100m, decreasing to undetectable concentrations by 200m (Haidar and Thierstein, 2001; Krumhardt et al., 2016). Okada and Honjo (1973a) published vertical profiles of coccolithophore concentrations in the top 200m for 19 stations along a transect from the subarctic to south central Pacific. Their results showed, almost without exception, decreases in coccolithophorids over the top 200m to levels about 10% of values seen shallower in the water column. In a meridional section across the Equatorial Pacific, stations closest to the equator showed the least vertical heterogeneity regarding coccolithophore abundance whereas off the equator, vertical heterogeneity increased as waters became more oligotrophic in character (Hagino et al., 2000). In the subantarctic South Atlantic (50-55°S, 37-42°W) subsurface coccolithophore maxima were clearly observed at depths of 50-80m (as observed by others (Boeckel and Baumann, 2008; Poulton et al., 2017; Poulton et al., 2006b)), belowwhich concentrations decreased.

It is tempting to conclude that the deep drop in abundance of calcite coccoliths and coccospheres at depths exceeding 200m, particularly under the NAG and SAG (Fig. 2E) was due to either: (1) grazing and conversion into fast-sinking fecal pellets (Baumann et al., 2014; Honjo, 1976) or (2) bio-induced dissolution in microaggregates or the guts of epi-pelagic zooplankton which are corrosive to calcite, despite the fact that such surface waters are still above the chemical lysocline and generally considered supersaturated for calcite (Harris, 1994; Milliman

Table 5

Ecological indices of diversity (H'), species richness (S) and Evenness (J') for surface and deep (fluorescence maximum) populations of coccolithophores. Cruise-wide means are given along with t-test results [two sample comparisons assuming unequal variances] for tstat; tcrit values and probability of accepting the null hypothesis (same mean values) when they are indeed different. Significantly different surface and deep values are indicated using bold face font

Index	Cruise	Mean surf	Mean deep	DF	t Stat	t crit (2-tailed)	P <
H'	AMT24	1.379	1.210	176	2.657	1.973	0.009
	AMT25	1.800	1.704	52	0.829	2.007	0.411
S	AMT24	4.190	3.397	230	2.687	1.970	0.008
	AMT25	7.559	6.971	64	0.533	1.998	0.596
J'	AMT24	1.104	1.108	179	-0.183	1.973	0.855
	AMT25	1.087	1.141	48	-2.245	2.011	0.029

et al., 1999; White et al., 2018). Other studies have shown strong decreases in PIC, coccospheres and coccoliths in the top 100-500m suggestive of aggregation, consumption and defecation, or dissolution through acid guts (Sherrell et al., 1998; Thomalla et al., 2008; Wollast and Chou, 1998). The calcite saturation state in the NAG and SAG ($\Omega_{\rm calc}$) at 300m depth is highly supersaturated but there is nonetheless evidence of dissolution above the carbonate saturation horizon (Chung et al., 2003).

4.2. Variability of nutrients and biogeochemical variables

The average nitrate sections were qualitatively and quantitatively similar to those published previously from other AMT cruises (Aiken et al., 2017; Hale et al., 2017; Painter et al., 2008; Poulton et al., 2006b; Robinson et al., 2006b). The section of mean dissolved inorganic phosphate also showed the same general spatial distribution as the nitrate distribution and was fully consistent with previous phosphate sections (Hale et al., 2017; Tsuchiya et al., 1992, 1994). The mean silicate section showed the same qualitative pattern to the other nutrients but, quantitatively, a deeper depth of the silicate nutricline than for nitrate and phosphate nutriclines, also observed by others (Tsuchiya et al., 1992, 1994).

The asymmetry in the nutrient sections of the North and South Subtropical Gyre were most pronounced for phosphate (Fig. 3B) where the NAG phosphate concentrations were, on average, drawn down more than in the SAG. The asymmetry was not as apparent in the mean nitrate section, which has been described previously (Robinson et al.,

Least-square linear fit relationships between the absolute value of latitude and diversity (H'), species richness (S) and evenness (J') for AMT cruises 24 and 25. Statistical significance of each relationship (last column) is given for two-tailed, alpha, type 1 error.

AMT Cruise	Independent variable (X)	Dependent variable (Y)	SE of dependent variable (Y)	Slope	SE of slope	Intercept	SE of intercept	r	DF	P <
24	Absolute latitude (deg)	H'	0.671	-0.0093	0.0039	1.358	0.126	0.212	122	0.05
24	Absolute latitude (deg)	S	0.3549	-0.0485	0.0206	5.458	0.669	0.208	122	0.05^{a}
24	Absolute latitude (deg)	J'	0.162	0.0028	0.0011	1.046	0.0338	0.252	99	0.05
25 ^a	Absolute latitude (deg)	S	3.446	-0.0771	0.0261	9.129	0.805	0.279	102	0.01

^a With one outlier removed, regression is not statistically significant.

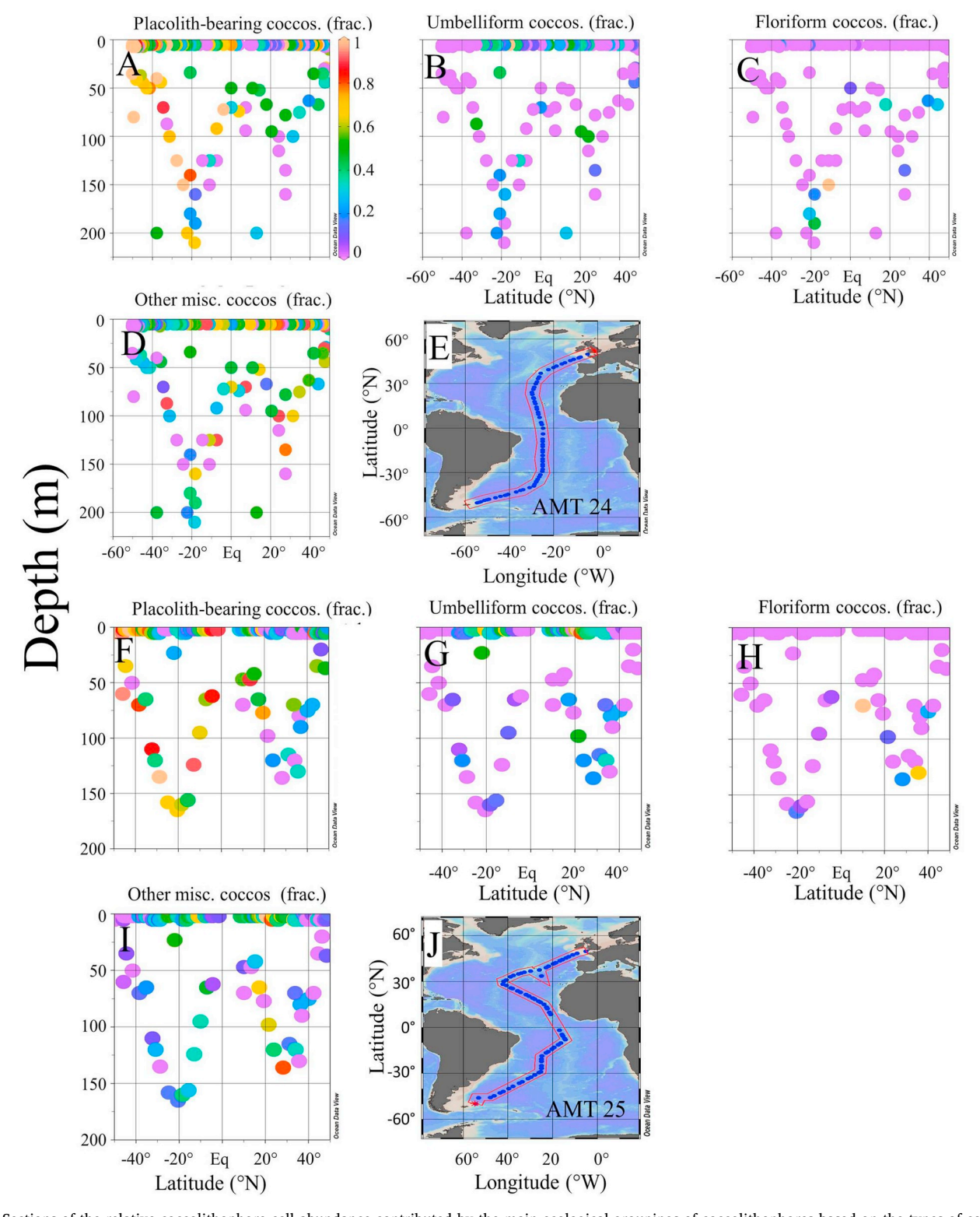


Fig. 9. Sections of the relative coccolithophore cell abundance contributed by the main ecological groupings of coccolithophores based on the types of coccoliths (Young, 1994), as observed in AMT24 and 25, respectively: (A,F) placolith-bearing, (B,G) umbelliform coccoliths, (C,H) floriform coccoliths, (D,I) other coccolithophore species not included in the first three categories above). (E, J) Cruise tracks of AMT24 and 25, respectively.

2006b). The lower phosphate concentrations in the NAG may indicate more nitrogen fixation occurring there (which alleviates nitrogen limitation, thus allowing more phosphate drawdown). This also allowed the nitrate:phosphate ratios to increase above the Redfield ratio at only 150m in the NAG as opposed to \sim 300m in the SAG (Fig. 3E). Residual nitrate distributions also showed a strong asymmetry between the NAG

and SAG where the depth of the zero value was at 150 and 250m, respectively (Fig. 3D). We caution that the data presented here are mostly from cruises during the northern hemisphere autumn, hence seasonal variability might complicate this interpretation. However, the CV values of residual nitrate at those depths in the SAG and NAG are low (Fig. 5D), so the asymmetry trend appears stable across this multiple

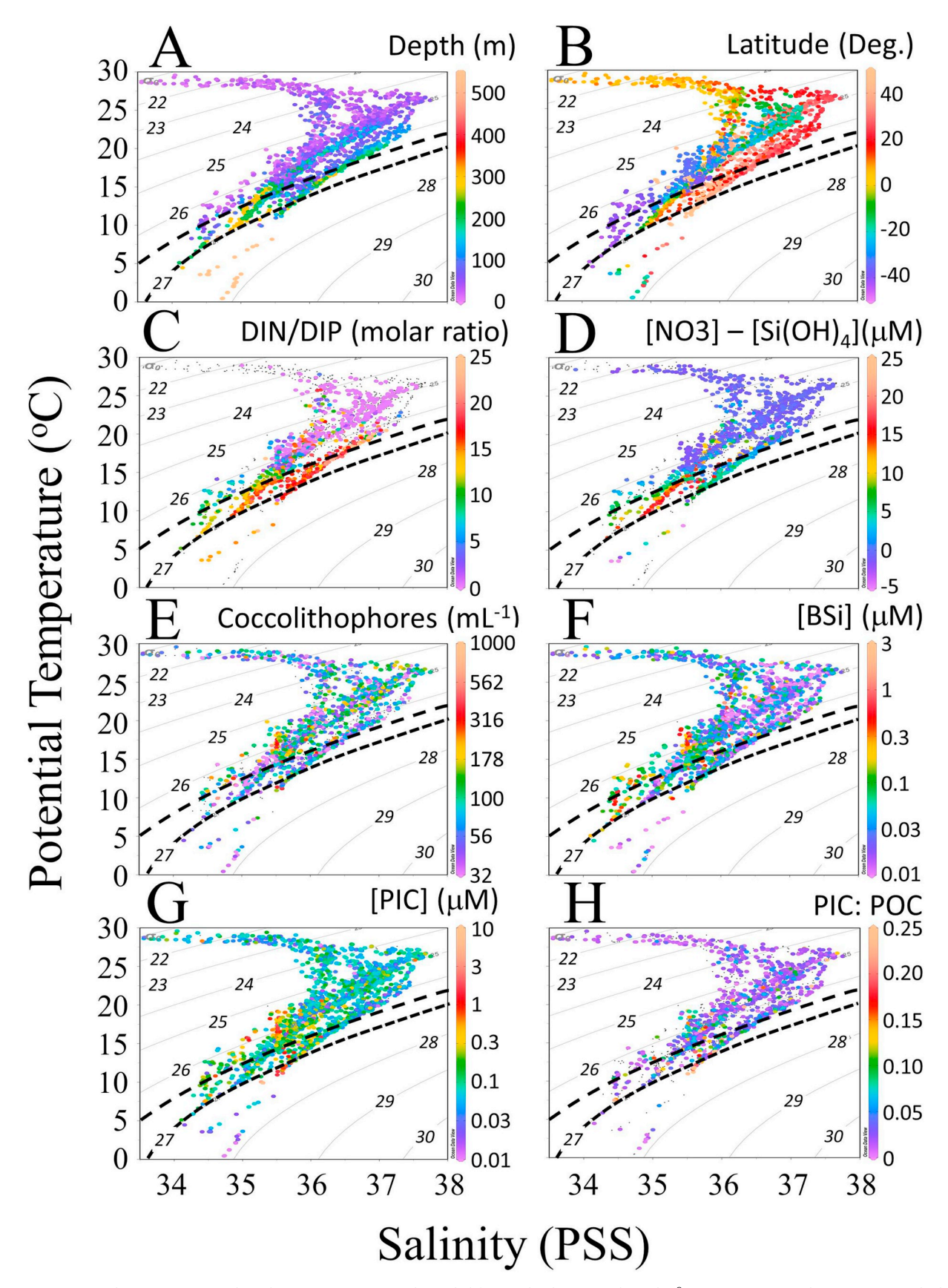


Fig. 10. Temperature-Salinity water mass plots along AMT transects, color coded for (A) depth (m), (B) latitude ($^{\circ}$ N), (C) DIN/DIP molar ratio, (D) residual nitrate (nitrate-silicate; μ M), (E) coccolithophore cell concentration ($^{\circ}$ L), (F) BSi (μ M), (G) PIC (μ M), and (H) PIC/POC ratio. Color keys given to the right of each panel. Density anomaly σ_0 contours shown as grey lines. Upper limit of SAMW is designated with a black long-dashed line. Deeper limit of SAMW is designated with a black short-dashed line.

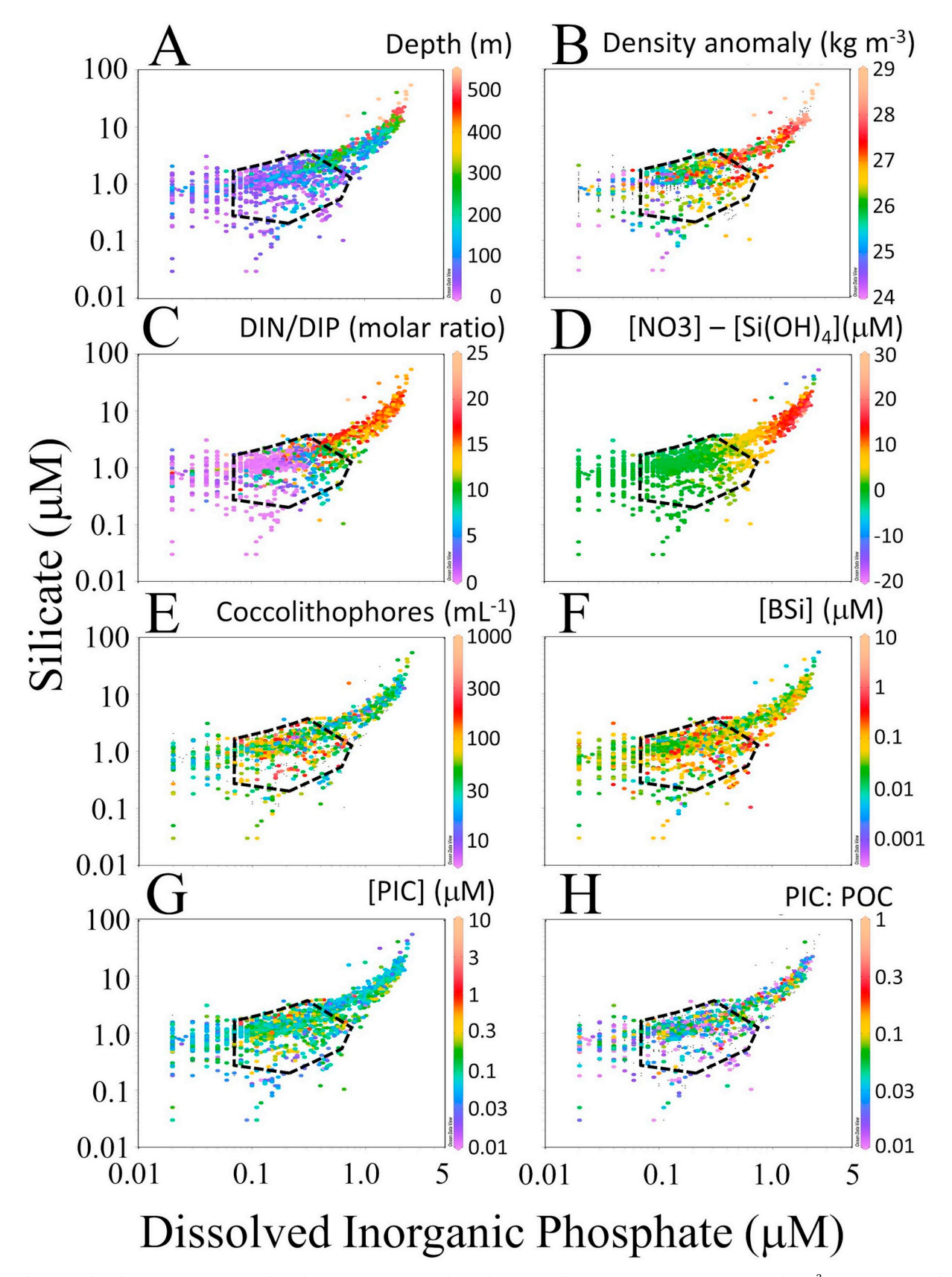


Fig. 11. Silicate vs phosphate concentration for data along AMT transects, color coded for (A) depth (m), (B) σ_0 density anomaly (kg m⁻³), (C) DIN/DIP molar ratio, (D) residual nitrate (nitrate-silicate; μ M), (E) coccolithophore cell concentration (mL⁻¹), (F) BSi (μ M), (G) PIC (μ M), and (H) PIC/POC ratio. Color keys given to the right of each panel. The silicate and phosphate concentrations where elevated coccolithophore concentrations were observed (100-1000 cells mL⁻¹) were enclosed within a polygon (drawn by eye in panel E) and the polygon was then transferred to other panels).

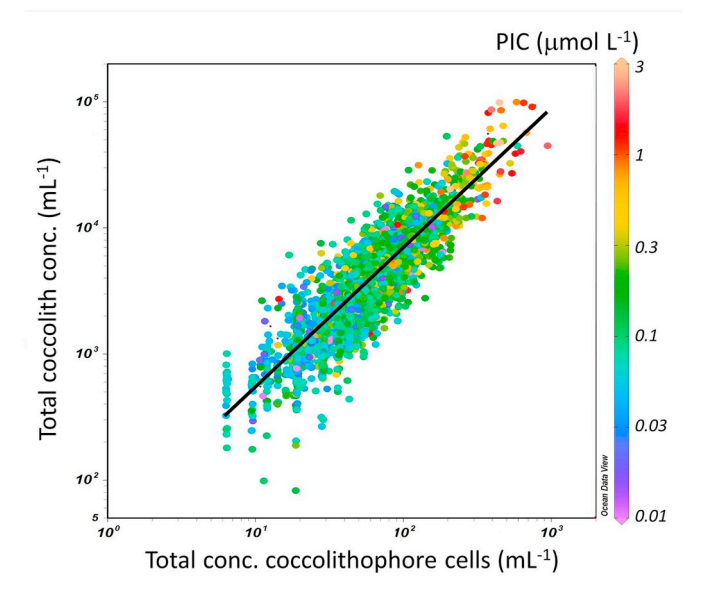


Fig. 12. Concentration of detached coccoliths (mL $^{-1}$) plotted against concentration of coccolithophore cells and aggregates (mL $^{-1}$). The concentration of PIC (μ M) is shown as the color of the dots. The least-squares, best-fit power function to these data is: (Log total coccolith[\pm 0.194 log units] = 38.603[\pm 1.711][Log total coccolithophore]^(1.1215[\pm 0.0107]); r^2 = 0.785; DF = 3039; F = 11,081; P < 0.001; values in square brackets are the standard error of each least-squares-fit coefficient). Note that the ratio of detached coccoliths to coccolithophore cells varies from 40, at low coccolithophore concentrations to 90 at highest concentrations.

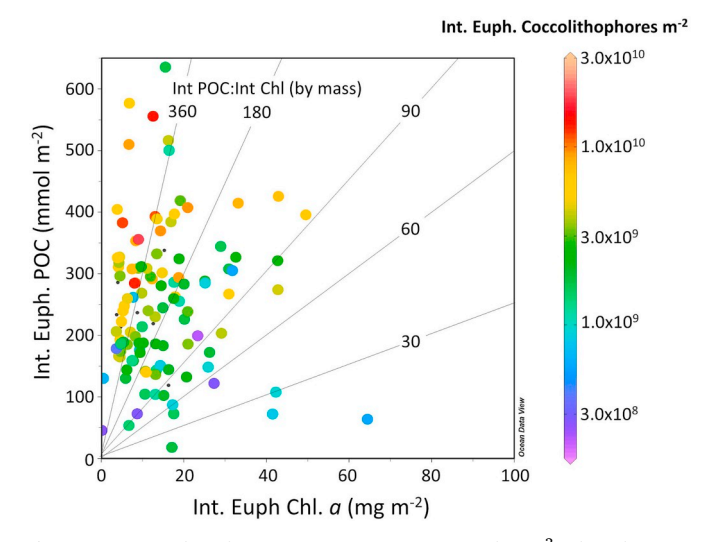


Fig. 13. Integrated euphotic POC concentration (mmoles m^{-2}) plotted against integrated euphotic chlorophyll concentration (mg m^{-2}). The color of the dots represents the integrated euphotic coccolithophore concentration. Isopleths of POC:chlorophyll mass ratios also are shown.

cruise data set. Such an asymmetry in the residual nitrate distribution likely affects the relative productivity of diatoms versus non-siliceous phytoplankton in the two subtropical gyres.

The interannual variance of the nutrient field (as quantified by the CV) was likely greatest in the gyres for the most limiting nutrient (Fig. 5). This is because, assuming a constant precision of each nutrient method, as the mean concentration of the limiting nutrient approached zero, the CV (standard deviation/mean) would have increased proportionately. The SAG showed the greatest CV for nitrate (5-10) as compared to a CV of 1-2 in the NAG (Fig. 5A), suggesting nitrate limitation in the SAG (or nitrate-iron co-limitation as suggested by

Browning et al. (2017)). Conversely, the interannual variability of the phosphate distributions were greatest in the NAG and EQ (CV =1-3) compared to CVs of 0.2-0.5 in the SAG (Fig. 5B), suggestive of phosphorous limitation in the NAG which has been promoted by others (McLaughlin et al., 2013; Salihoglu et al., 2008; Wu et al., 2000).

PIC distributions (Fig. 2A) were fully consistent with other basin scale estimates of PIC from other AMT cruises (Poulton et al., 2007). The same was true for comparisons of mean surface PIC concentrations with satellite PIC estimates, based on the NASA PIC ocean color algorithm, which showed highest surface PIC concentrations in the STW where elevated concentrations of coccolithophores are associated with the Great Calcite Belt (GCB) or NTW where high concentrations of coccolithophores are also commonly reported (Balch et al., 2005, 2016; Holligan et al., 1993; Hopkins et al., 2015). CVs for PIC suggested the most interannual variability in the NTW, not the STW/GCB. This may simply be due to the more ephemeral appearance of coccolithophore blooms in the NTW, especially during the sampling period of the AMT cruises (late northern hemisphere fall). The mean BSi section (Fig. 2C), which showed relatively homogeneous concentrations over the top 300m in the STW, EQ and NTW, illustrates that these waters are regions of strong silica export. Such export patterns have been described based on sediment trap data (as well as models derived from sediment trap data) (Honjo et al., 2008).

The average chlorophyll *a* section (Fig. 2D) for the cruises sampled here (Table 2) was highly similar to patterns observed from other AMT cruises (Aiken et al., 2017; Poulton et al., 2006a; Robinson et al., 2006b), and again, the interannual variance was greatest in the gyres (Fig. 4D). There was relatively poor coherence between the chlorophyll *a* and POC sections, though (Fig. 2B,D) which likely resulted from photoadaption of the deep phytoplankton (hence increased chlorophyll:carbon ratios at depth) but also, the POC likely included significant fractions of non-living organic carbon associated with heterotrophic bacteria, zooplankton, detritus, etc., which would have lowered the coherence with chlorophyll (Fig. 2B) (Gundersen et al., 2001; Poulton et al., 2007). Presumably, the high interannual variability of POC was associated with variability in the vertical transformations of POC over the top 300m, as well (Thomalla et al., 2008).

4.3. Coccolithophore species assemblages and their variability

The relatively invariant background concentration of detached coccoliths in the upper 300m of the water column was striking. Such stable concentrations could be due to relatively constant production rates combined with slow loss rates. For example, detached coccoliths sink at velocities of 0.14m d⁻¹ (Honjo, 1976) while plated coccolithophore cells sink about 10X faster (1.3m d⁻¹; (Eppley et al., 1967)). The majority of the detached coccoliths (when they were present) were from the ubiquitous species, *E. huxleyi* (Fig. 6G), which also would have contributed to the relatively invariant background concentrations.

The most abundant coccolithophore species was E. huxleyi, seen throughout both AMT 24 and 25 (Fig. 6) with increasing relative abundance with increasing latitude. This was wholly consistent with the prior observations of McIntyre and Be (1967), who showed E. huxleyi to be the most (or second-most) abundant species for their subarctic, subantarctic and bordering transitional regions (McIntyre and Be (1967), see their table 10). Indeed, E. huxleyi was noted to be present in each of the five floral assemblages described by McIntyre and Be (1967): subarctic, subantarctic, transitional, subtropical and tropical. Others have also shown increasing dominance of E. huxleyi with increasing latitudes (Holligan et al., 2010; Poulton et al., 2017). Other common coccolithophores such as U. tenuis and U. irregularis were described to have the highest relative abundance in subtropical and tropical regions, respectively (McIntyre and Be, 1967); this was also observed in our results (Fig. 6B and C). Our results, and those of Poulton et al. (2017) (for different AMT cruises, #12 and #14), show these species to be most abundant in the upper euphotic zone (see their table 8; Table S2), although there were clear cases where U. tenuis was observed in the DCM (Fig. 6B, H). While G. oceanica rarely surpassed 20% of the coccolithophore floral assemblage in AMT 24 and 25, overall, it was present, at an average relative abundance of $\sim 1\%$ of the total coccolithophore assemblage and showed strong patchiness, our results, again, were consistent with McIntyre and Be (1967) who showed G. oceanica to be present in tropical, subtropical and transitional floral assemblages. Poulton et al. (2017) classified this species as rare and McIntyre and Be (1967) classified this species to be < 1% of the total flora in these biogeographic zones. D. tubifera was included in McIntyre and Be (1967) description as being a surface dwelling species in tropical and subtropical floral groups which was generally consistent with our observations (Fig. 6E,K) except we observed clear cases of this species in the DCM in AMT25 (Fig. 6K).

Along with comparing the distributions of individual species, we also addressed the similarity of the entire coccolithophore floral assemblages with those described by McIntyre and Be (1967). Their table 10 lists the coccolithophore species that made up the floral assemblages for tropical, subtropical, transitional, subarctic and subantarctic regions. We compared each of our species assemblages to their floral assemblages, calculating a qualitative index of similarity based on species presence or absence. The comparison was based on the fraction of each assemblage that we found that was in common with McIntyre and Be (1967) list. For example, if we qualitatively observed the exact same species assemblage observed by McIntyre and Be (1967), the sample would be scored a 1. If we observed half the species of a given McIntyre and Be (1967) assemblage, it would be scored as 0.5. If we observed other species to be "diluting" the McIntyre and Be (1967) assemblage (i.e. species not on their list), the assemblage score was decreased accordingly by the fractional makeup of those other nonlisted species.

Using this index, we typically observed samples with less than half of the species assemblages in common with the McIntyre and Be (1967) lists (typically a maximum of 20-30% for any given geographic domain), and there was considerable overlap geographically (Fig. S5). For example, we found samples in the subtropics that showed 20-30% of the species in common with McIntyre and Be's tropical assemblage, and vice versa. This was true for both AMT 24 and AMT25 results (Figs. S5A and B; S5G, H). The transitional assemblages were indeed observed near the poleward end of the subtropical domains but these, too, showed overlap with the subtropical assemblages. The surface and deep patterns also did not necessarily covary (Fig. S5). Most noteworthy however, was the fraction of the Subantarctic assemblage with 40-50% scores south of 40°S (Fig. S5C). Moreover, McIntyre and Be's subantarctic floral assemblage was observed in the DCM of the subtropics and tropics, showing scores of 40-50% similarity. To the extent that floral assemblages match the waters from which they originated, this is consistent with the subduction of SAMW northwards along the density surface at the base of the euphotic zone (Fig. S5C). The E. huxleyi morphotypes also conveyed this pattern, with the Type C cells (typically most common in the Southern Ocean (Young et al., 2003)), sporadically found in the DCM of both hemispheres (Fig. S6C) (Saavedra-Pellitero

The deep coccolithophore species observed in the DCM below 100m in the SAG during AMT 24 and 25 (*F. profunda*, *R. clavigera*, *M. adriaticus*, *C. murrayi* and *U. foliosa*; Fig. 7) were somewhat different than the profiles described by Boeckel and Baumann (2008) (*F. profunda*, *Gephyrocapsa ericsonii*, *Oolithotus antillarum*, *Oolithotus fragilis*) or those described by Baumann et al. (2008) (*Calcidiscus leptoporus*, *F. profunda*, *Oolithotus* sp., and *U. sibogae*). The species that we observed were a subset of the species observed by Poulton et al. (2017) for lower and sub-euphotic depths. What is consistent is that these coccolithophores growing near depths of 200m in the SAG would be close to the depth of the nitracline (Fig. 3A) and clearly close to the limits of light-limited photosynthesis (see also Fig. 9 showing the distribution of the floriform grouping of coccolithophores, as defined by Young (1994)).

Nonetheless, the DCM samples from the AMT cruises typically fall around the 1% light depth (base of the mixed layer) (Poulton et al., 2017) at the base of the euphotic zone, which is at the limits of autotrophic growth. While not definitive, mixotrophic life strategies for these and deeper populations might provide a selective advantage (Aubry, 2009). These deep species would also reside in SAMW and would be modifying it in its northward transit from its source in the Southern Ocean.

4.4. Coccolithophore diversity and ecological groupings

The higher diversity of the coccolithophore assemblages in the top 50m as compared to the DCM is comparable to results seen by others, at least in the South Atlantic (Boeckel and Baumann, 2008). Moreover, the highest species richness was observed in the SAG (for both cells and detached coccoliths), also observed previously (Boeckel and Baumann, 2008; McIntyre and Be, 1967; Okada and Honjo, 1973b; Poulton et al., 2017). Species richness estimates from this study were lower than those described by Poulton et al. (2017), who also sampled from other AMT cruises. This was likely due to the lower effective volume of water examined in our samples (0.88 mL) compared to the 15mL samples used by Poulton et al. (2017). Poulton et al. showed with rarefaction curves that increasing the volume viewed by a factor of four in the same sample, approximately doubled the number of species observed (see Fig. 3 of Poulton et al., 2017). Thus, a priori, we would have expected our richness estimates to be ~4X lower than Poulton et al. (2017), missing the rarest species, which indeed was the case.

There also were statistically significant inverse relationships of diversity with the absolute value of latitude (Table 4), which has been suggested by others (O'Brien et al., 2016; Poulton et al., 2017; Righetti et al., 2019). Species evenness showed the opposite pattern; at high latitudes, species were more evenly distributed among the fewer species present, whereas at low latitudes, there was the tendency to have a few dominants along with rare species among the diverse assemblages. This is opposite to the trend showed by Poulton et al.(2017). Thus, there was both lower diversity and richness in high-latitude waters, which also showed the highest PIC, coccolithophore and coccolith concentrations (Figs. 2, 8, S1, S4). The tendency towards elevated diversity at lower latitudes is not unique just to coccolithophores but is seen in other planktonic phyla such as tintinnids and foraminifera (Dolan et al., 2006; Rutherford et al., 1999).

4.5. Implications for ocean color

This trend of lower diversity for the coccolithophore species that detach their coccoliths, compared to the overall coccolithophore diversity has ramifications for their optical properties. Algorithms that are currently used to estimate PIC are fundamentally backscattering algorithms (Balch et al., 2005; Mitchell et al., 2017), reliant on an average PIC-specific backscattering cross-section, which for the original PIC algorithms was predominantly derived from one species, E. huxleyi, because it causes massive blooms (Balch et al., 1996a, 1996b, 1999). Moreover, detached coccoliths are typically 40-90X more concentrated than the plated coccolithophore cells that produce them (Fig. 12) and their typical < 3um diameter gives them peak scattering cross-sections (Balch et al., 1996a). Detached coccoliths, therefore, play a disproportionate role in the backscattering signal of suspended PIC as seen by ocean color satellites. At high coccolithophore concentrations such as in a bloom, the proportion of reflectance originating from the optically-active detached coccoliths will more than double (Fig. 12). Moreover, the backscattering cross-sections of individual coccoliths will depend on the morphology of the coccoliths which will vary by species (Gordon and Du, 2001; Neukermans and Fournier, 2018). In short, a reduced diversity of detached coccoliths means that there will be less morphological variability for the highly optically-active, detached coccoliths, hence less variability in the PIC-specific backscattering cross

section. Thus, PIC algorithms will be more reliable for converting optical backscattering to the concentration of PIC (Balch, 2018) at high latitudes with greater PIC concentrations, where *E. huxleyi* dominates. At lower latitudes with lower PIC concentrations, however, there will be a higher coccolithophore diversity with different coccolith morphologies and less reliable conversion of optical backscattering to PIC. The one optical study involving a variety of coccolithophore species other than *E. huxleyi*, showed higher PIC-specific backscattering cross-sections (Balch et al., 1999).

4.6. SAMW and controls on coccolithophores

What is most striking about the coccolithophore distributions seen across the north and south Atlantic, over all of the cruises, is that the lowest surface coccolithophore and PIC concentrations were consistently observed in the EQ (lower than even the subtropical gyres; Fig. 2A), where biogenic silica (an indicator of diatom biomass) was moderately elevated in the EQ (Fig. 2C). Bishop et al. (1977) also observed similarly low PIC concentrations in the equatorial Atlantic. Poulton et al. (2017) also commented on the low abundance of coccospheres in EQ waters as observed over two AMT cruises, where the highest coccosphere numbers were recorded from temperate waters (> 30°S) and the lowest from equatorial waters. The question is whether this was bottom-up control (by nutrients) or top-down control (by grazing). If it is bottom-up control, then the question is what is the ultimate source of the nutrients for the phytoplankton populations of the EQ upwelling region of the Atlantic? Thus, do the low concentrations of coccolithophores in the equatorial Atlantic result from an inability of coccolithophores to grow in upwelled SAMW there? If the situation is caused by top-down control, then the question is what predators are selectively consuming the coccolithophores. This is a fertile area for future study.

Our analysis of the different variables associated with the different water masses (Fig. 10) suggests that regions of elevated PIC, coccolithophore cells and BSi (basically, most of the biomineralizing phytoplankton classes) in the STW were associated with SAMW or waters just above it. Moreover, these regions had increased PIC:POC ratios. The SAMW, regardless of whether it was in the north or south Atlantic, was characterized by the DIN/DIP ratio closer to the Redfield ratio, conducive to general phytoplankton growth. Equatorial waters showed silicate upwelling shallower than the 26 σ_{θ} isopycnal (above the SAMW) which was likely the cause of the BSi peak seen over the top 300m of the water column of the EQ (Fig. 2C).

The association of peaks of coccolithophores, diatoms (as BSi) and PIC in SAMW (Fig. 10E, F, G) was also seen when the data were plotted according to nutrient chemistry (Fig. 11). That is, peaks in coccolithophores and diatoms (BSi) were mostly seen in waters within (or above) the SAMW (Fig. 11) that showed moderately low silicate and phosphate as well as waters that were shallower than 150m (Fig. 11A). The high diatom abundance would have drawn down the silicate levels. Moreover, waters shallower than 150m would have been at the base of the euphotic zone, thus, suggesting a possible light connection in the nutrient drawdown. These waters were characterized by Redfield ratios at or below 16 (Fig. 11C) and residual nitrate values that were zero to slightly positive, so nitrate was in excess (Fig. 11D). Notably, when PIC and BSi were plotted against each other, there was no statistically significant relationship between them (results not shown). This indicates that neither biomineralizing algal class in these low nutrient waters was responding to the same stimulus, contrary to Barber and Hiscock's, "a rising tide lifts all phytoplankton" (Barber and Hiscock, 2006). We can only conclude that there are other factors that are allowing one biomineralizing algal class to dominate the other in these nutrient stressed situations, factors such as top-down grazing, or bottom-up limitation or co-limitation by another nutrient, trace metal or vitamin. See also Nissen et al.(2018) for more discussion on this based on a modeling exercise in the Southern Ocean.

4.7. Coccolithophore-diatom competition

The coccolithophores of the GCB (Balch et al., 2011a) may be preconditioning this SAMW (just as the diatoms have been suggested to do, by drawing down the silicate in SAMW before it is subducted) (Sarmiento et al., 2004). Such coccolithophore preconditioning would increase the pCO₂, draw down alkalinity, as well as other trace metals or cofactors required for coccolithophore growth (Balch et al., 2016). It remains an open question whether this preconditioning is what is keeping the equatorial Atlantic coccolithophore populations at such low levels when this SAMW upwells at the EQ some 40 years later. A similar phenomenon might happen in the Pacific, too. While coccolithophores are indeed observed in equatorial Pacific waters, bright coccolithophore blooms are not (Balch and Kilpatrick, 1996; Balch et al., 2011b; Okada and Honjo, 1973a). Blooms of large diatoms are observed in equatorial Pacific waters, which ultimately may be outcompeting coccolithophores there, especially in areas of fertilization by iron and silicate (Brzezinski et al., 2011; Yoder et al., 1994).

Both iron and silicate are important in the competition between diatoms and coccolithophores (Balch et al., 2016; Brzezinski et al., 2011). Previous observations from the equatorial Pacific waters showed that both chlorophyll and bulk PIC increased in a statistically significant fashion, associated with equatorial upwelling, (Balch et al., 2011b) but that diatoms and coccolithophores varied inversely in controlled microcosm experiments where silica, iron and germanium (an inhibitor of diatom cell division) were added (Brzezinski et al., 2011). Coccolithophores there did not respond to iron addition (suggesting that they were not limited by iron, unlike the large diatoms) whereas, when relieved of competition by diatoms (by silicate limitation or germanium addition), coccolithophores flourished. Similar competitive relationships between diatoms and coccolithophores have been hypothesized in the GCB (Balch et al., 2016; Nissen et al., 2018); the presence of silicate meant that diatom growth could be maintained at high rates, but when silicate levels dropped below ~2 uM (Paasche, 1973a, b), the remainder of the phytoplankton community could maintain their growth in high-nutrient-low-chlorophyll (HNLC) waters. However, under conditions where diatoms were growth-limited for silicate and iron, coccolithophores were able to out-compete picophytoplantkon, nanophytoplankton and dinoflagellates (Balch et al., 2016), forming high-reflectance blooms visible from ocean color satellites.

4.8. PIC fluxes and the carbonate versus silicate ocean concept

In the global sediment trap database of Honjo et al. (2008), vertical fluxes of PIC, associated with equatorial upwelling, are some of the highest measured, in the mid-Pacific equatorial waters and eastern equatorial Pacific. There were somewhat lower PIC fluxes in the eastern equatorial Atlantic (Honjo et al., 2008). Observation of elevated PIC fluxes in equatorial waters combined with our observations of reduced coccolithophore standing stocks there appear to be contradictory unless the downward flux of PIC at 1-3.5km depth is dominated by other calcifiers such as pteropods and foraminfera. Our AMT PIC sampling protocol would have been unlikely to include PIC from foraminifera and pteropods since the sample volumes were < 0.5 liters and the numerical abundance of foraminifera and pteropods is typically several per liter or several per cubic meter, respectively, thus their appearance in our PIC samples would have been stochastic, at best. Therefore, our observations would be consistent with the conclusion of Sarmiento et al. (2002) that any elevated PIC:POC export ratios in equatorial waters are due to foraminifera- and pteropod-associated calcite fluxes, not coccolithophore fluxes.

Honjo et al. (2008) described the "silica ocean" and the "carbonate ocean" as a way to quantify the predominant source of ballast for the flux of sinking POC. That is, when the molar ratio of the POC:PIC fluxes or BSi/PIC fluxes is < 1 then this is deemed the carbonate ocean. When these ratios are > 1 then this is deemed a "silica ocean". Using these

criteria, about 80% of the world ocean is considered to be a "carbonate ocean", particularly dominated by the oligotrophic subtropical gyres (Honjo et al., 2008). Indeed, while the POC:chlorophyll ratio increases in oligotrophic regions in surface waters (Rasse et al., 2017), we, too, saw that highest euphotic zone-integrated concentrations of coccolithophore cells were associated with waters with elevated euphotic POC:euphotic chlorophyll ratios, in a predictable fashion, across multiple cruises (Fig. 13). This is the first time this has been demonstrated over such a large geographical area as the Atlantic Basin and over a multi-year time period. This directly supports the carbonate ocean concept of Honjo et al. (2008).

4.9. Concluding remarks

The results of these AMT cruises show highest abundances of coccolithophores with communities of low diversity, low species richness, and high evenness (more evenly distributed species among the fewer species present) in the NTW and particularly the STW. Indeed, there is a high abundance of the placolith-bearing coccolithophore species, E. huxleyi, particularly apparent in the GCB, found in the STW and the Subantarctic Front. The presence of deep euphotic and sub-euphotic coccolithophore populations in the SAG and NAG provide tantalizing suggestion that these deep-dwelling species of coccolithophores may be heterotrophic and/or mixotrophic (see also Poulton et al. (2017)). Moreover, the placolith-bearing, umbelliform and floriform coccolithophore species are growing in the SAMW pycnostad, originally formed at the Subantarctic front, then subducted equatorwards (Cerovečki et al., 2013). The grand question remains as to why the equatorial Atlantic is so low in coccolithophore abundance, when it is generally considered productive for other phytoplankton groups such as diatoms? We hypothesize that the placolith-bearing coccolithophores of the GCB as well as the deep floriform coccolithophores are preconditioning the SAMW before and after it is subducted northward, and that affects which phytoplankton can thrive in that water when it upwells at the equator decades later. This hypothesis could be addressed through the application of marine ecosystem models (which can address both top-down and bottom-up controls) or through systematic examination of the SAMW source waters along with controlled experiments to define the factors that affect coccolithophore growth and loss. Ultimately, the results will have ramifications to our understanding of the chemistry (alkalinity balance, nutrient balance, productivity) of both the SAMW and equatorial waters, as well as basinscale primary production.

Acknowledgements

NASA was the primary supporter of the research described herein (NAS5-31363, NNG04HZ25C; NNX11AL93G; NNX14AQ43A, NNX17AI77G, 80NSSC19K0043). Support was also provided by NSF (OCE-1735664). Data used for this paper are stored in the NASA-SEABASS data archive (http://seabass.gsfc.nasa.gov/) and in the UK BODC (https://www.bodc.ac.uk/data/published data library/ catalogue/10.5285/8a046e6e-2b12-683f-e053-6c86abc09d82/). thank the Atlantic Meridional Transect program of the UK for allowing us to participate on their cruises. Malcolm Woodward (Plymouth Marine Laboratory) was responsible for the nutrient results presented here. The Atlantic Meridional Transect is funded by the UK Natural Environment Research Council through its National Capability Longterm Single Centre Science Programme, Climate Linked Atlantic Sector Science (grant number NE/R015953/1). This study contributes to the international IMBeR project and is contribution number 336 of the AMT programme. We thank M. Saavedra-Pellitero and several other anonymous reviewers who provided thoughtful reviews of earlier drafts of this manuscript.

Appendix A. Supplementary data

Supplementary data to this article can be found online at https://doi.org/10.1016/j.dsr.2019.06.012.

References

- Aiken, J., Brewin, R.J.W., Dufois, F., Polimene, L., Hardman-Mountford, N.J., Jackson, T., Loveday, B., Hoya, S.M., Dall'Olmo, G., Stephens, J., Hirata, T., 2017. A synthesis of the environmental response of the North and South Atlantic Sub-Tropical Gyres during two decades of AMT. Prog. Oceanogr. 158, 236–254.
- Andreé, K., 1920. Geologie des Meeresbodens. Borntraeger, Leipzig.
- Aubry, M.P., 2009. A sea of Lilliputians. Palaeogeogr. Palaeoclimatol. Palaeoecol. 284 (1-2), 88–113.
- Balch, W., Utgoff, P., 2009. Potential interactions among ocean acidification, coccolithophores and the optical properties of seawater. Oceanography 22 (4), 146–159.
 Balch, W.M., 2018. The ecology, biogeochemistry, and optical properties of coccolithophores. Annual Review of Marine Science 10, 71–98.
- Balch, W.M., Bates, N.R., Lam, P.J., Twining, B.S., Rosengard, S.Z., Bowler, B.C., Drapeau, D.T., Garley, R., Lubelczyk, L., Mitchell, C.E., Rauschenberg, S., 2016. Factors regulating the Great calcite Belt in the Southern Ocean and its biogeochemical significance. Glob. Biogeochem. Cycles. https://doi.org/10.1002/2016GB005414.
- Balch, W.M., Bowler, B.C., Drapeau, D.T., Lubelczyk, L.C., Lyczkowski, E., 2018. Vertical distributions of coccolithophores, PIC, POC, biogenic silica, and chlorophyll a throughout the global ocean. Glob. Biogeochem. Cycles 32 (1). https://doi.org/10. 1002/2016GB005614.
- Balch, W.M., Drapeau, D.T., Bowler, B.C., Booth, E.S., Lyczskowski, E., Alley, D., 2011a. The contribution of coccolithophores to the optical and inorganic carbon budgets during the Southern Ocean Gas Experiment: new evidence in support of the "Great Calcite Belt" hypothesis. Journal of Geophysical Research-Special Issue 116, 1–14.
- Balch, W.M., Drapeau, D.T., Cucci, T.L., Vaillancourt, R.D., Kilpatrick, K.A., Fritz, J.J., 1999. Optical backscattering by calcifying algae–Separating the contribution by particulate inorganic and organic carbon fractions. J. Geophys. Res. 104, 1541–1558.
- Balch, W.M., Fabry, V.J., 2008. Ocean acidification: documenting its impact on calcifying phytoplankton at basin scales. Mar. Ecol. Prog. Ser. 373, 239–247.
- Balch, W.M., Gordon, H.R., Bowler, B.C., Drapeau, D.T., Booth, E.S., 2005. Calcium carbonate budgets in the surface global ocean based on MODIS data. Journal of Geophysical Research Oceans 110 (C7), C07001 07010.01029/02004JC002560.
- Balch, W.M., Kilpatrick, K., Holligan, P.M., Harbour, D., Fernandez, E., 1996a. The 1991 coccolithophore bloom in the central north Atlantic. II. Relating optics to coccolith concentration. Limnol. Oceanogr. 41, 1684–1696.
- Balch, W.M., Kilpatrick, K.A., 1996. Calcification rates in the equatorial Pacific along 140°W. Deep Sea Research II 43, 971–993.
- Balch, W.M., Kilpatrick, K.A., Holligan, P.M., Trees, C., 1996b. The 1991 coccolithophore bloom in the central north Atlantic. I. Optical properties and factors affecting their distribution. Limnol. Oceanogr. 41, 1669–1683.
- Balch, W.M., Poulton, A.J., Drapeau, D.T., Bowler, B.C., Windecker, L., Booth, E., 2011b. Zonal and meridional patterns of phytoplankton biomass and carbon fixation in the Equatorial Pacific Ocean, between 110°W and 140°W. Deep-Sea Research II 58 (3-4), 400–416.
- Barber, R.T., Hiscock, M.R., 2006. A rising tide lifts all phytoplankton: growth response of other phytoplankton taxa in diatom-dominated blooms. Glob. Biogeochem. Cycles 20 (4).
- Barrett, P.M., Resing, J.A., Grand, M.M., Measures, C.I., Landing, W.M., 2018. Trace element composition of suspended particulate matter along three meridional CLIVAR sections in the Indian and Southern Oceans: impact of scavenging on Al distributions. Chem. Geol. 502, 15–28. https://doi.org/10.1016/j.chemgeo.2018.06.015.
- Barton, A.D., Dutkiewicz, S., Flierl, G., Bragg, J., Follows, M.J., 2010. Patterns of diversity in marine phytoplankton. Science 327 (5972), 1509–1511.
- Baumann, K.-H., Bockel, B., Frenz, M., 2004. Coccolith contribution to South Atlantic carbonate sedimentation. In: Thierstein, H.R., Young, J.R. (Eds.), Coccolithophores from Molecular Processes to Global Impact. Springer-Verlag, Heidelberg, pp. 368–402.
- Baumann, K.-H., Boeckel, B., Čepek, M., 2008. Spatial distribution of living coccolithophores along an eastwest transect in the subtropical South Atlantic. J. Nannoplankt. Res. 30 (1), 9–21.
- Baumann, M.S., Moran, S.B., Lomas, M.W., Kelly, R.P., Bell, D.W., Krause, J.W., 2014. Diatom control of the autotrophic community and particle export in the eastern Bering sea during the recent cold years (2008–2010). J. Mar. Res. 72 (6), 405–444.
- Bibby, T.S., Moore, C.M., 2011. Silicate:nitrate ratios of upwelled waters control the phytoplankton community sustained by mesoscale eddies in sub-tropical North Atlantic and Pacific. Biogeosciences 8, 657–666.
- Bishop, J.K.B., Edmond, J.M., Ketten, D.R., Bacon, M.P., Silker, W.B., 1977. The chemistry, biology, and vertical flux of particulate matter from the upper 400 m of the equatorial Atlantic Ocean. Deep Sea Res. 24 (6), 511–548.
- Boeckel, B., Baumann, K.H., 2008. Vertical and lateral variations in coccolithophore community structure across the subtropical frontal zone in the South Atlantic Ocean. Mar. Micropaleontol. 67 (3-4), 255–273.
- Browning, T.J., Achterberg, E.P., Rapp, I., Engel, A., Bertrand, E.M., Tagliabue, A., Moore, C.M., 2017. Nutrient co-limitation at the boundary of an oceanic gyre. Nature 551 (7679), 242–246.
- Brzezinski, M., Baines, S.B., Balch, W.M., Beucher, C.P., Chai, F., Dugdale, R.C., Krause, J.W., Landry, M.R., Marchi, A., Measures, C.I., Nelson, D.M., Parker, A.E., Poulton, A.J., Selph, K., Strutton, P.G., Taylor, A.G., Twining, B.S., 2011. Co-limitation of

- diatoms by iron and silicic acid in the equatorial Pacific. Deep-Sea Research II 58, 493–511.
- Brzezinski, M.A., Nelson, D.M., 1989. Seasonal changes in the silicon cycle within a Gulf Stream warm-core ring. Deep Sea Res. I 36, 1009–1030.
- Campbell, J.W., 1995. The lognormal distribution as a model for bio-optical variability in the sea. J. Geophys. Res. 100 (C7), 13237–13254.
- Cerovečki, I., Talley, L.D., Mazloff, M.R., Maze, G., 2013. Subantarctic mode water formation, destruction, and export in the eddy-permitting southern ocean state estimate. J. Phys. Oceanogr. 43 (7), 1485–1511.
- Cheng, Z., Zheng, Y., Mortlock, R., Van Geen, A., 2004. Rapid multi-element analysis of groundwater by high-resolution inductively coupled plasma mass spectrometry. Anal. Bioanal. Chem. 379 (3), 512–518.
- Chisholm, S.W., Olson, R.J., Zettler, E.R., Goericke, R., Waterbury, J., Welschmeyer, N., 1988. A novel free-living prochlorophyte abundant in the oceanic euphotic zone. Nature 334, 340–343.
- Chung, S.-N., Lee, K., Feely, R.A., Sabine, C.L., Millero, F.J., Wanninkhof, R., Bullister, J.L., Key, R.M., Peng, T.-H., 2003. Calcium carbonate budget in the Atlantic Ocean based on water column inorganic carbon chemistry. Glob. Biogeochem. Cycles 17 (4) 4-1 to 4-15
- Conrad, W., 1941. Sur les Chrysomonadines à trois fouets. Aperçu synoptique. Bull. Musee R. Hist. Nat. Belg. 17, 1–16.
- Cortés, M.Y., Bollmann, J., Thierstein, H.R., 2001. Coccolithophore ecology at the HOT station ALOHA, Hawaii. Deep-Sea Res. Part II Top. Stud. Oceanogr. 48 (8-9), 1957–1981
- Deflandre, G., Fert, C., 1952. Sur la structure fine de quelque coccolithes fossiles observers au microscope electronique signification morphogenetique et application systematique. C. r. hebd. Seanc. Acad. Sci., Paris 234, 2100–2102.
- Deflandre, G., Fert, C., 1954. Observations sur les coccolithophoridrs actuals et fossilesen microscopic ordinaire et electronique. Ann. Paleontol. 40, 117–176.
- Demarest, M.S., Brzezinski, M.A., Nelson, D.M., Krause, J.W., Jones, J.L., Beucher, C.P., 2011. Net biogenic silica production and nitrate regeneration determine the strength of the silica pump in the Eastern Equatorial Pacific. Deep-Sea Res. Part II Top. Stud. Oceanogr. 58 (3-4), 462–476.
- Dolan, J.R., Lemée, R., Gasparini, S., Mousseau, L., Heyndrickx, C., 2006. Probing diversity in the plankton: using patterns in Tintinnids (planktonic marine ciliates) to identify mechanisms. Hydrobiologia 555 (1), 143–157.
- Eppley, R.W., Holmes, R.W., Strickland, J.D.H., 1967. Sinking rates of marine phytoplankton measured with a fluorometer. J. Exp. Mar. Biol. Ecol. 1, 191–208.
- Fournier, G., Neukermans, G., 2017. An analytical model for light backscattering by coccoliths and coccospheres of *Emiliania huxleyi*. Optic Express 25 (13), 14996–15009.
- Gaarder, K.R., 1954. Coccolithineae, silicoflagellatae, pterospermataceae and other forms from the Michael Sars North Atlantic Deep-Sea expedition 1910. Rep. scicnt. Results Michael Sars N. Atlant. Deep-Sea Exped. 2 (4), 20.
- Goldstein, J., Newbury, D., Joy, D., Lyman, C., Echlin, P., Lifshin, E., Sawyer, L., Michael, J., 2003. Scanning Electron Microscopy and X-Ray Microanalysis. Springer Science + Business Media, LLC, New York.
- Gordon, H.R., Du, T., 2001. Light scattering by nonspherical pariticles: application to coccoliths detached from *Emiliania huxleyi*. Limnol. Oceanogr. 46 (6), 1438–1454.
- Green, J.C., Leadbeater, B.S.C. (Eds.), 1994. The Haptophyte Algae. Clarendon Press, Oxford.
- Gundersen, K., Orcutt, K.M., Purdieb, D.A., Michaels, A.F., Knap, A.H., 2001. Particulate organic carbon mass distribution at the Bermuda Atlantic Time-series Study (BATS) site. Deep Sea Res. Part II 48, 1697–1718.
- Hagino, K., Okada, H., Matsuoka, H., 2000. Spatial dynamics of coccolithophore assemblages in the equatorial western-central pacific ocean. Mar. Micropaleontol. 39, 53–72.
- Haidar, A.T., Thierstein, H.R., 2001. Coccolithophore dynamics off Bermuda (N. Atlantic). Deep Sea Res. 48 (8-9), 1925–1956.
- Haidar, A.T., Thierstein, H.R., Deuser, W.G., 2000. Calcareous phytoplankton standing stocks, fluxes and accumulation in Holocene sediments off Bermuda (N. Atlantic). Deep Sea Res. 47 (9-11), 1907–1938.
- Hale, M.S., Li, W.K.W., Rivkin, R.B., 2017. Meridional patterns of inorganic nutrient limitation and co-limitation of bacterial growth in the Atlantic Ocean. Prog. Oceanogr. 158, 90–98.
- Harris, R.P., 1994. Zooplankton grazing on the coccolithophore *Emiliania huxleyi* and its role in inorganic carbon flux. Mar. Biol. 119, 431–439.
- Holligan, P.M., Charalampopoulou, A., Hutson, R., 2010. Seasonal distributions of the coccolithophore, *Emiliania huxleyi*, and of particulate inorganic carbon in surface waters of the Scotia Sea. J. Mar. Syst. 82 (4), 195–205.
- Holligan, P.M., Fernandez, E., Aiken, J., Balch, W., Boyd, P., Burkill, P., Finch, M., Groom, S., Malin, G., Muller, K., Purdie, D., Robinson, C., Trees, C., Turner, S., van der Wal, P., 1993. A biogeochemical study of the coccolithophore, *Emiliania huxleyi*, in the north Atlantic. Glob. Biogeochem. Cycles 7 (4), 879–900.
- Honjo, S., 1976. Coccoliths: production, transportation and sedimentation. Mar. Micropaleontol. 1, 65–79.
- Honjo, S., Manganini, S.J., Krishfield, R.A., Francois, R., 2008. Particulate organic carbon fluxes to the ocean interior and factors controlling the biological pump: a synthesis of global sediment trap programs since 1983. Prog. Oceanogr. 76 (3), 217–285.
- Honjo, S., Okada, H., 1974. Community structure of coccolithophores in the photic layer of the mid-Pacific. Micropaleontology 20 (2), 209–230.
- Hopkins, J., Henson, S.A., Painter, S.C., Tyrrell, T., Poulton, A.J., 2015. Phenological characteristics of global coccolithophore blooms. Glob. Biogeochem. Cycles 29 (2), 239–253.
- Houdan, A., Probert, I., Zatylny, C., Véron, B., Billard, C., 2006. Ecology of oceanic coccolithophores. I. Nutritional preferences of the two stages in the life cycle of

- Coccolithus braarudii and Calcidiscus leptoporus. Aquat. Microb. Ecol. 44 (3), 291–301.
 Jordan, R.W., Kleijne, A., 1994. A classification system for living coccolithophores. In:
 Winter, A., Siesser, W. (Eds.), Coccolithphores. Oxford University Press, Cambridge, pp. 242.
- Kirkwood, D.S., 1989. Simultaneous Determination of Selected Nutrients in Seawater. International Council for the Exploration of the Seas Copenhagen, Denmark.
- Krumhardt, K.M., Lovenduski, N.S., Freeman, N.M., Bates, N.R., 2016. Apparent increase in coccolithophore abundance in the subtropical North Atlantic from 1990 to 2014. Biogeosciences 13 (4), 1163–1177 1110.5194/bg-1113-1163-2016.
- Leibold, M.A., Hall, S.R., Smith, V.H., Lytle, D.A., 2017. Herbivory enhances the diversity of primary producers in pond ecosystems. Ecology 98 (1), 48–56.
- Li, L., Chesson, P., 2016. The effects of dynamical rates on species coexistence in a variable environment: the paradox of the plankton revisited. Am. Nat. 188 (2), F46-F58
- Liu, H., Probert, I., Uitz, J., Claustre, H., Aris-Brosou, S., Frada, M., Not, F., 2009. Extreme diversity in noncalcifying haptophytes explains a major pigment paradox in open oceans. Proc. Natl. Acad. Sci. U.S.A. 106 (31), 12803–12808.
- Lohmann, H., 1902. Die Coccolithophoridae, eine Monographie der Coccolithenbilenden Flagellaten, zugleich ein Beitrag zur Kenntnis des Mittelmeerauftriebs. Arch. Protistenkd. 1, 89–165.
- Lohmann, H., 1908. On the relationship between pelagic deposits and marine plankton. Int. Rev. Gesamten Hydrobiol. 1, 309–323.
- Magurran, A.E., 2004. Meausuring Biological Diversity. Blackwell Science, Ltd., Malden, MA USA.
- McCartney, M.S., 1982. The subtropical recirculation of mode waters. J. Mar. Res. 40 (Suppl. l), 427–464.
- McGowan, J.A., Walker, P.W., 1993. Pelagic diversity patterns. In: Ricklefs, R.E., Schluter, D. (Eds.), Species Diversity in Ecological Communities. University of Chicago Press, Chicago, Illinois, pp. 203–214.
- McIntyre, A., Be, A.W.H., 1967. Modern coccolithophoridae of the Atlantic Ocean. I. Placoliths and cyrtoliths. Deep Sea Res. 14, 561–597.
- McLaughlin, K., Sohm, J.A., Cutter, G.A., Lomas, M.W., Paytan, A., 2013. Phosphorus cycling in the Sargasso Sea: investigation using the oxygen isotopic composition of phosphate, enzyme-labeled fluorescence, and turnover times. Glob. Biogeochem. Cycles 27 (2), 375–387.
- Medlin, L.K., Sáez, A.G., Young, J.R., 2008. A molecular clock for coccolithophores and implications for selectivity of phytoplankton extinctions across the K/T boundary. Mar. Micropaleontol. 67, 69–86.
- Menden-Deuer, S., Rowlett, J., 2014. Many ways to stay in the game: individual variability maintains high biodiversity in planktonic microorganisms. J. R. Soc. Interface 11 (95)
- Milliman, J.D., Troy, P.J., Balch, W.M., Adams, A.K., Li, Y.H., Mackenzie, F.T., 1999.
 Biologically mediated dissolution of calcium carbonate above the chemical lysocline?
 Deep-Sea Res. Part I Oceanogr. Res. Pap. 46 (10), 1653–1669.
- Mitchell, C., Hu, C., Bowler, B., Drapeau, D., Balch, W.M., 2017. Estimating particulate inorganic carbon concentrations of the global ocean from ocean color measurements using a reflectance difference approach. J. Geophys. Res.: Oceans 122 (11), 8707–8720
- Moshkovitz, S., Osmond, K., 1989. The optical properties and microcrystallography of Arkhangelskiellaceae and some other calcareous nannofossils in the Late Cretaceous. In: Crux, J.A., van Heck, S.E. (Eds.), Nannofossils and Their Applications. Ellis Horwood, Chichester, pp. 76–97.
- Neukermans, G., Fournier, G., 2018. Optical modeling of spectral backscattering and remote sensing reflectance from *Emiliania huxleyi* Blooms. Frontiers in Marine Science 5 (MAY).
- Nissen, C., Vogt, M., Münnich, M., Gruber, N., Alexander Haumann, F., 2018. Factors controlling coccolithophore biogeography in the Southern Ocean. Biogeosciences 15 (22), 6997–7024.
- O'Brien, C.J., Vogt, M., Gruber, N., 2016. Global coccolithophore diversity: drivers and future change. Prog. Oceanogr. 140, 27–42.
- Okada, H., Honjo, S., 1973a. Distribution of Coccolithophorids in the North and Equatorial Pacific Ocean: Quantitative Data on Samples Collected during Leg 30, OSHORO MARU, 1968 and LEG HK69-4, HAKUHO MARU, 1969. Woods Hole Oceanographic Institution, Woods Hole, pp. 1–58.
- Okada, H., Honjo, S., 1973b. The distribution of oceanic coccolithophorids in the Pacific. Deep-Sea Res. 20, 355–374.
- Okada, \dot{H} ., McIntyre, A., 1977. Modern coccolithophores of the Pacific and North Atlantic Oceans. Micropaleontology 23, 1–55.
- Okada, H., McIntyre, A., 1979. Seasonal distribution of modern coccolithophores in the western North Atlantic Ocean. Mar. Biol. 54, 319–328.
- Paasche, E., 1973a. Silicon and the ecology of marine plankton diatoms. II. Silicate-up-take kinetics in five diatom species. Mar. Biol. 19, 262–269.
- Paasche, E., 1973b. Silicon and the ecology of marine planktonic diatoms. 1. *Thalassiosira pseudonana* (*Cyclotella nana*) grown in chemostats with silicate as the limiting nutrient. Mar. Biol. 19, 117–126.
- Painter, S.C., Sanders, R., Waldron, H.N., Lucas, M.I., Woodward, E.M.S., Chamberlain, K., 2008. Nitrate uptake along repeat meridional transects of the Atlantic Ocean. J. Mar. Syst. 74 (1-2), 227–240.
- Parsons, T.R., Maita, Y., Lalli, C.M., 1984. A Manual of Chemical and Biological Methods for Seawater Analysis. Pergamon Press Inc., New York.
- Pintner, I.J., Provasoli, L., 1968. Heterotrophy in subdued light of 3 Chrysochromlina species. Bull. Misaki Mar. Biol. Inst. Kyoto Univ. 12, 25–31.
- Poole, R., Tomczak, M., 1999. Optimum multiparameter analysis of the water mass structure in the Atlantic Ocean thermocline. Deep-Sea Res. Part I Oceanogr. Res. Pap. 46 (11), 1895–1921.
- Poulton, A., Holligan, P., Hickman, A., Kim, Y.-N., Adey, T.R., Stinchcombe, M.C.,

- Holeton, C., Root, S., Woodward, M.S., 2006a. Phytoplankton carbon fixation, chlorophyll-biomass and diagnostic pigments in the Atlantic Ocean. Deep -Sea Research II 53, 1593–1610.
- Poulton, A.J., Adey, T.R., Balch, W.M., Holligan, P.M., 2007. Relating coccolithophore calcification rates to phytoplankton community dynamics: regional differences and implications for carbon export. Deep-Sea Res II Chapman Calcification Conference-Special 54 (5-7), 538-557.
- Poulton, A.J., Holligan, P.M., Charalampopoulou, A., Adey, T.R., 2017. Coccolithophore ecology in the tropical and subtropical Atlantic Ocean: new perspectives from the Atlantic Meridional Transect (AMT) programme. Prog. Oceanogr. https://doi.org/10. 1016/j.pocean.2017.1001.1003.
- Poulton, A.J., Sanders, R., Holligan, P.M., Adey, T., Stinchcombe, M., Brown, L., Chamberlain, K., 2006b. Phytoplankton mineralisation in the tropical and subtropical Atlantic Ocean. Glob. Biogeochem. Cycles 20 (4), GB4002 4010.1029/ 2006/58002712
- Poulton, A.J., Young, J.R., Bates, N.R., Balch, W.M., 2011. Biometry of detached *Emiliania huxleyi* coccoliths along the patagonian shelf. Mar. Ecol. Prog. Ser. 443, 1–17.
- Rasse, R., Dall'Olmo, G., Graff, J., Westberry, T.K., van Dongen-Vogels, V., Behrenfeld, M.J., 2017. Evaluating optical proxies of particulate organic carbon across the surface Atlantic Ocean. Frontiers in Marine Science 4 (367). https://doi.org/10.3389/fmars. 2017.00367
- Redfield, A.C., Ketchum, B.H., Richards, F.A., 1963. The influence of organisms on the composition of sea-water. In: Hill, M.N. (Ed.), The Sea. Wiley, New York, pp. 26–77.
- Riebesell, U., Kortzinger, A., Oschlies, A., 2009. Sensitivities of marine carbon fluxes to ocean change. Proc. Natl. Acad. Sci. U.S.A. 106 (49), 20602–20609.
- Righetti, D., Vogt, M., Gruber, N., Psomas, A., Zimmermann, N.E., 2019. Global pattern of phytoplankton diversity driven by temperature and environmental variability. Science Advances 5 (5).
- Robinson, C., Holligan, P., Jickells, T., 2006a. The Atlantic meridional transect programme. Deep-Sea Res. Part II Top. Stud. Oceanogr. 53 (14-16), 1483–1484.
- Robinson, C., Poulton, A.J., Holligan, P.M., Baker, A.R., Forster, G., Gist, N., Jickells, T.D., Malin, G., Upstill-Goddard, R., Williams, R.G., Woodward, E.M.S., Zubkov, M.V., 2006b. The Atlantic meridional transect (AMT) programme: a contextual view 1995-2005. Deep-Sea Res. Part II Top. Stud. Oceanogr. 53 (14-16), 1485–1515.
- Rutherford, S., D'Hondt, S., Prell, W., 1999. Environmental controls on the geographic distribution of zooplankton diversity. Nature 400 (6746), 749–753.
- Saavedra-Pellitero, M., Baumann, K.H., Flores, J.A., Gersonde, R., 2014. Biogeographic distribution of living coccolithophores in the Pacific sector of the Southern Ocean. Mar. Micronaleontol. 109, 1–20.
- Salihoglu, B., Garçon, V., Oschlies, A., Lomas, M.W., 2008. Influence of nutrient utilization and remineralization stoichiometry on phytoplankton species and carbon export: a modeling study at BATS. Deep-Sea Res. Part I Oceanogr. Res. Pap. 55 (1), 73–107.
- Sarmiento, J.L., Dunne, J., Gnanadesikan, A., Key, R.M., Matsumoto, K., Slater, R., 2002.

 A new estimate of the CaCO₃ to organic carbon export ratio. Glob. Biogeochem.

 Cycles 16 (4), 1107.
- Sarmiento, J.L., Gruber, N., Brzezinski, M.A., Dunne, J.P., 2004. High-latitude controls of thermocline nutrients and low latitude biological productivity. Nature 427, 56–60.
- Schlitzer, R., 2018. Ocean Data view. http://odv.awi.de.
- Sherrell, R.M., Field, M.P., Gao, Y., 1998. Temporal variability of suspended mass and composition in the Northeast Pacific water column: relationships to sinking flux and lateral advection. Deep-Sea Research II 45, 733–761.

- Sloyan, B.M., Rintoul, S.R., 2001. Circulation, renewal, and modification of Antarctic Mode and Intermediate Water. J. Phys. Oceanogr. 31 (4), 1005–1030.
- Taylor, A.R., Brownlee, C., Wheeler, G., 2017. Coccolithophore cell biology: chalking up progress. Annual Review of Marine Science 9 (1), 283–310.
- Thierstein, H., Cortes, M.Y., Haidar, A.T., 2004. Plankton community behavior on ecological and evolutionary time-scales: when models confront evidence. In: Thierstein HR, Young JR (Eds.), Coccolithophores- from Molecular Processes to Global Impact. Springer, Berlin, Germany, pp. 455–479.
- Thierstein, H.R., Young, J.R. (Eds.), 2004. Coccolithophores-from Molecular Processes to Global Impact. Springer-Verlag, Berlin.
- Thomalla, S.J., Poulton, A.J., Sanders, R., Turnewitsch, R., Holligan, P.M., Lucas, M.I., 2008. Variable export fluxes and efficiencies for calcite, opal, and organic carbon in the Atlantic Ocean: a ballast effect in action? Glob. Biogeochem. Cycles 22 (GB1010). https://doi.org/10.1029/2007GB002982.
- Townsend, D.W., Keller, M.D., Holligan, P.M., Ackleson, S.G., Balch, W.M., 1994. Blooms of the coccolithophore *Emiliania huxleyi* with respect to hydrography in the Gulf of Maine. Cont. Shelf Res. 14 (9), 979–1000.
- Townsend, D.W., Rebuck, N.D., Thomas, M.A., Karp-Boss, L., Gettings, R.M., 2010. A changing nutrient regime in the Gulf of Maine. Cont. Shelf Res. 30, 820–832.
- Tsuchiya, M., Talley, L.D., McCartney, M.S., 1992. An eastern Atlantic section from Iceland southward across the equator. Deep Sea Res. Part A, Oceanographic Research Papers 39 (11-12), 1885–1917.
- Tsuchiya, M., Talley, L.D., McCartney, M.S., 1994. Water-mass distributions in the western South Atlantic; A section from South Georgia Island (54S) northward across the equator. J. Mar. Syst. 52, 55–81.
- Waterbury, J.B., Watson, S.W., Guillard, R.R.L., Brand, L.E., 1979. Widespread occurrence of a unicellular, marine, planktonic, cyanobacterium. Nature 277 (5694), 202, 204
- White, M.M., Waller, J.D., Lubelczyk, L.C., Drapeau, D.T., Bowler, B.C., Balch, W.M., Fields, D.M., 2018. Coccolith dissolution within copepod guts affects fecal pellet density and sinking rate. Sci. Rep. 8 (1), 9758.
- Winter, A., Siesser, W.G. (Eds.), 1994. Coccolithophores. Cambridge University Press, Cambridge.
- Wollast, R., Chou, L., 1998. Distribution and fluxes of calcium carbonate along the continental margin in the Gulf of Biscay. Aguat. Geochem. 4 (3-4), 369–393.
- Woodward, E.M.S., Rees, A.P., 2001. Nutrient distributions in an anticyclonic eddy in the northeast Atlantic ocean, with reference to nanomolar ammonium concentrations. Deep-Sea Res. Part II Top. Stud. Oceanogr. 48 (4-5), 775–793.
- Wu, J., Sunda, W., Boyle, E.A., Karl, D.M., 2000. Phosphate depletion in the western North Atlantic ocean. Science 289 (5480), 759–762.
- Yoder, J.A., Ackleson, S.G., Barber, R.T., Flament, P., Balch, W.M., 1994. A line in the sea.

 Nature 371, 689–692.
- Young, J.R., 1994. Functions of coccoliths. In: Winter, A., Siesser, W.G. (Eds.), Coccolithophores. Cambridge University Press, Cambridge, U.K., pp. 63–82.
- Young, J.R., Cros, L., Kleijne, A., Sprengel, C., Probert, I., Østergaard, J.B., 2003. A guide to extant coccolithophore taxonomy. Journal of Nannoplankton Research Special Issue 1, 1–121.
- Ziveri, P., Baumann, K.-H., Böckel, B., Bollmann, J., Young, J.R., 2004. Biogeography of selected holocene coccoliths in the Atlantic Ocean. In: Thierstein, H.R., Young, J.R. (Eds.), Coccolithophores: from Molecular Processes to Global Impact. Springer-Verlag, Berlin Heidelberg, pp. 403–428.